NAVAL POSTGRADUATE SCHOOL
MONTEREY, CALIFORNIA

THESIS

NAVY OPERATIONAL GLOBAL ATMOSPHERIC PREDICTION SYSTEM (NOGAPS) ANALYSIS AND FORECAST CHARACTERISTICS OF EXTRATROPICAL CYCLOLYSIS OVER THE NORTH PACIFIC OCEAN

by

Thomas Paul Wojahn

June, 1996

Thesis Co-Advisors: Paul A. Hirschberg
                          Patrick A. Harr

Approved for public release; distribution is unlimited.

19961008 193

1. AGENCY USE ONLY *(Leave blank)*	2. REPORT DATE June, 1996	3. REPORT TYPE AND DATES COVERED Master's Thesis
4. TITLE AND SUBTITLE: NAVY OPERATIONAL GLOBAL ATMOSPHERIC PREDICTION SYSTEM (NOGAPS) ANALYSIS AND FORECAST CHARACTERISTICS OF EXTRATROPICAL CYCLOLYSIS OVER THE NORTH PACIFIC OCEAN.		5. FUNDING NUMBERS
6. AUTHOR(S) Wojahn, Thomas P.		
7. PERFORMING ORGANIZATION NAME(S) AND ADDRESS(ES) Naval Postgraduate School Monterey CA 93943-5000		8. PERFORMING ORGANIZATION REPORT NUMBER
9. SPONSORING/MONITORING AGENCY NAME(S) AND ADDRESS(ES)		10. SPONSORING/MONITORING AGENCY REPORT NUMBER
11. SUPPLEMENTARY NOTES The views expressed in this thesis are those of the author and do not reflect the official policy or position of the Department of Defense or the U.S. Government.		
12a. DISTRIBUTION/AVAILABILITY STATEMENT Approved for public release; distribution is unlimited.		12b. DISTRIBUTION CODE

13.   ABSTRACT *(maximum 200 words)*

   Simulations with high resolution air/sea coupled models and several case studies have lead to the hypothesis that friction parameterizations could have a profound affect on the accuracy of numerical analysis and prediction of decaying cyclones. In this study, analyzed and forecast characteristics of decaying cyclones over the North Pacific Ocean are related to the hypothesized importance of friction induced cyclone spin down. Many characteristics of cyclolysis, which include gale area size and decay rate, were found to vary according to the synoptic-scale conditions in which the cyclone exists. Furthermore, the hypothesized relationship between cyclolysis and frictionally forced spin down was not found to exist in the analyzed and forecast model data. This result might be expected since friction spin down is parameterized based on analyzed and forecast winds over synoptic space and time scales. Therefore, it is concluded that over these scales other factors, which may include energy transfers due to barotropic processes, contribute in a major way to cyclone decay as portrayed in a global-scale numerical model.

14. SUBJECT TERMS NOGAPS, Cyclolysis, Friction parameterization				15. NUMBER OF PAGES 77
				16. PRICE CODE
17. SECURITY CLASSIFICATION OF REPORT Unclassified	18. SECURITY CLASSIFICATION OF THIS PAGE Unclassified	19. SECURITY CLASSIFICATION OF ABSTRACT Unclassified		20. LIMITATION OF ABSTRACT UL

NAVY OPERATIONAL GLOBAL ATMOSPHERIC PREDICTION SYSTEM (NOGAPS) ANALYSIS AND FORECAST CHARACTERISTICS OF EXTRATROPICAL CYCLOLYSIS OVER THE NORTH PACIFIC OCEAN

Thomas Paul Wojahn
Lieutenant, United States Coast Guard
B.S., United States Coast Guard Academy, 1989

Submitted in partial fulfillment
of the requirements for the degree of

MASTER OF SCIENCE IN METEOROLOGY AND PHYSICAL OCEANOGRAPHY
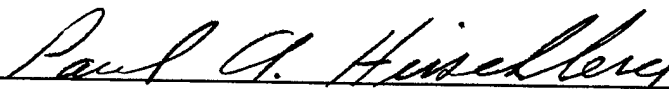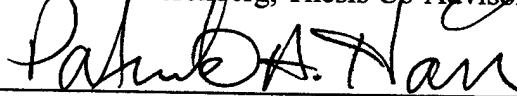
from the

NAVAL POSTGRADUATE SCHOOL
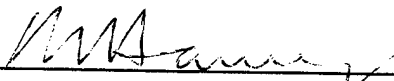June 1996

Author:_____

Thomas Paul Wojahn

Approved by:_____

Paul A. Hirschberg, Thesis Co-Advisor

_____

Patrick A. Harr, Thesis Co-Advisor

_____

Robert L. Haney, Chairman
Department of Meteorology

ABSTRACT

Concentrated research has lead to improved understanding and prediction of extratropical cyclone development. Little research has been done on cyclolysis even though the decaying portion of a cyclone's life cycle, which begins after maximum intensity, poses maritime operational conerns. Numerical simulations with high resolution coupled air/sea models and several detailed case studies have lead to the hypothesis that friction parameterizations could have a profound affect on the accuracy of numerical analysis and prediction of decaying cyclones. In this study, analyzed and forecast characteristics of decaying cyclones over the North Pacific Ocean are related to the hypothesized importance of friction-induced cyclone spin down. It is found that many observed and forecast characteristics of cyclolysis, including gale area size and decay rate, vary according to the synoptic-scale conditions in which the cyclone exists. Furthermore, no evidence is found for the hypothesized relationship between cyclolysis and frictionally forced spin down in the analyzed and forecast model data. This result might be expected since friction spin down is parameterized based on analyzed and forecast winds over synoptic space and time scales. Therefore, it is concluded that over these scales other factors, which may include energy transfers due to barotropic processes, contribute in a major way to cyclone decay as portrayed in a global-scale numerical model.

TABLE OF CONTENTS

I. INTRODUCTION

There has been a great amount of research done on extratropical cyclones (e.g. Newton and Holopainen 1990; Gronas and Shapiro 1994). This work has aided the development of sophisticated numerical models that can now accurately simulate cyclogenesis (e.g., Mullen and Smith 1990; Grumm 1993), even rapidly developing events over the oceans (e.g., Sanders, 1986; Sanders and Auciello 1989; Sanders 1992) on an operational basis. However, while much effort has been successfully directed towards understanding and improving the prediction of the development portion of the cyclone life cycle, not much consideration has been given to the decay stage. In particular, only a few of the studies that document cyclone characteristics (e.g., Petterssen 1956; Klein 1957; Reitan 1974; Whittaker and Horn 1981) specifically examine the characteristics of cyclolysis. Zishka and Smith (1980) constructed observed cyclolysis distributions over North America for the period 1950 to 1977. They found two prominent regions of cyclone decay along the Pacific coast of Canada and the northwestern U.S. and in a region extending from Pennsylvania and New York to the Hudson Bay. Gyakum et al. (1989) looked at North Pacific cold-season cyclone activity from 1975 through 1983 and found significant zones of dissipation to be located in the Gulf of Alaska and west of the Kamchatka peninsula. They also found a relatively high percentage of dissipating cyclones that had previously developed rapidly (Sanders and Gyakum, 1980) to be located in the region west and north of the Aleutians.

There has also been little theoretical treatment of cyclolysis aside from some idealized numerical studies of nonlinear baroclinic wave life cycles (e.g., Simons 1972;

Gall 1976; Simmons and Hoskins, 1979, 1980) that have shown the importance of barotropic processes as baroclinic waves occlude. The lack of attention to filling cyclones may have left numerical models with inadequate physics, such as friction parameterizations (e.g., Doyle, 1995), to properly simulate storms that are filling, but nevertheless, are still near the peak of their intensity. Besides simply extending the range of predictability, and providing important information for climate models (Simmons and Hoskins, 1980), more accurate numerical simulation of decaying cyclones would enable better assessment of accompanying weather phenomena such as high winds and precipitation. An improvement in the prediction of filling storms over the oceans would be especially significant since these storms can still pose major hazards to Navy and civilian maritime interests.

Three general model forecast errors that can be gleaned from the paucity of studies that have directly addressed forecast error statistics during cyclolysis are that models tend to move and fill storms too slowly and track them north and west of observed tracks. Mullen and Smith (1993) examined sea-level cyclone forecasts produced by the Nested-Grid Model (NGM) and the Aviation Run (AVN) of the T80 Global Spectral Model (GSM) over North America and adjacent ocean regions for two cool seasons. They found that filling storms were over forecasted by the NGM, and under forecasted by the AVN (see also Grumm and Siebers, 1990). More recently, Grumm (1993) found the T126 version of the GSM to fill filling cyclones too slowly. Harr et al. (1992) examined the Navy Operational Global Atmospheric Prediction System (NOGAPS; Hogan and Rosmond, 1991) forecasts of cyclones over the North Pacific. They found the largest negative central pressure errors (forecast pressure lower than observed) and negative track errors (forecast position left of the actual track) to occur over the climatological regions

2

of cyclone dissipation in the Sea of Okhotsk, east of the Kamchatka Peninsula, and the Gulf of Alaska.

In this thesis, the decay characteristics of analyzed and predicted extratropical cyclones over the North Pacific Ocean in the NOGAPS is examined. The study period is over the fourteen cool season months from January 1994 through February 1996, after the most recent major upgrade to the NOGAPS model. The thesis is organized as follows: An overview of cyclogenesis and the mechanisms of cyclolysis is provided in Chapter II. The data and methodology for this study is described in Chapter III. The results are presented in Chapters IV and a summary, conclusions and recommendations for future research is given in Chapter V.

4

II. BACKGROUND

The Norwegian cyclone model (Bjerknes 1919; Bjerknes and Solberg 1921; 1922) provides the foundation for our understanding of the development and evolution of extratropical cyclones. According to this four stage model (Figure 2.1), cyclones form, evolve and dissipate along fronts or narrow transitions zones that separate air masses with contrasting properties such as temperature and moisture (Figure 2.1a). Disturbances originate as small perturbations and as they develop potential energy which is due to the juxtaposition of warm and cold air masses, is transferred to storm kinetic energy by the uplift of the "warm sector" air that resides between the cold and warm fronts, and the sinking of colder air on the other sides of these fronts (Figure 2.1b). The disturbance intensifies as the cold front advances faster than the warm front with the pressure at the cyclone center decreasing and the circulation about it increasing (Figure 2.1c). As the cold front overtakes the warm front at first near the cyclone center an "occluded" front forms (Figure 2.1d). Gradually, the area of warm-sector air is reduced as it is lifted above the advancing cold air and the reservoir of potential energy that drives the storm is depleted and removed further from the cyclone center. When the cyclone becomes cutoff from its warm sector and potential energy is no longer available, the cyclone stops deepening and begins to fill owing to friction. Thereafter, the cold front overtakes the warm front at increasing distances form the cyclone center, the occlusion lengthens, and the cyclone is transformed in a large cold vortex in the lower troposphere with warm air still existing higher up (Figure 2.1e). The whole process comes to an end when the

5

cyclone ultimately takes on the character of a barotropic whirl, which loses its frontal character and gradually dissipates.

Over the years, modifications of the Norwegian model have been made as networks of upper-air observations, the formulations of quasi-geostrophic theory and baroclinic instability theory, and the advent of computers and numerical models enabled clearer insights about the dynamics of cyclones. For example, Carlson (1994) presents a modern Norwegian or "dynamic" cyclone model that includes important upper-level processes. According to this model, cyclogenesis can be understood in terms of a geostrophic adjustment, self-development process that involves the interplay between upper-level vorticity advection and lower-level temperature or thickness advection with important contributions from diabatic heating at times. Specifically, upper-level positive vorticity advection and the associated divergence downstream from an upper-level short-wave trough deepens surface cyclone centers, while the subsequent increased low-level temperature advection intensifies the upper-level vorticity advection by sharpening the upper-level trough and downstream ridge.

Hoskins et al. (1985) frame cyclogenesis in terms of the evolution of tropopause- and surface-based potential vorticity (PV) anomalies (Figure 2.2). From the standpoint of this conceptualization, cyclones are the result of the superposition of two circulations that are "induced" (Davis and Emmanuel, 1991) or "attributed" (Bishop and Thorpe, 1994) to the upper and lower PV anomalies that are initially horizontally offset. Hirschberg and Fritsch (1991a,b) discuss the important hydrostatic role that temperature anomalies associated with tropopause undulations or PV anomalies play in cyclogenesis. According to their model (Figure 2.3), the surface low center is always located under the warmest

6

column of air. During the initial stages of cyclogenesis, the surface low is underneath warm tropospheric air and the relatively high and cold portion of a tropopause undulation. As self-development continues, lower-stratospheric warm advection acts to deepen the low, while upstream subsidence intensifies the stratospheric warm pool that accompanies the low portion of the tropopause undulation. This upper-level warming hydrostatically forces the low to move increasingly underneath the stratospheric warm pool and towards an occluded configuration. The cyclone reaches its maximum intensity when the low is directly underneath the warmest stratospheric layer.

In these dynamic models of cyclogenesis, cyclones become occluded when the three-dimensional trough system including the surface low is more or less vertically aligned or "stacked" and the necessary upper-level forcing for continued deepening has moved well downstream. Unlike the original Norwegian model, the role of the fronts is more or less passive and the process of occlusion is not due to frontal movement but rather, is produced by a rearrangement of mass brought about by dynamic processes (Carlson, 1994). With the deepening process over, the occluded cyclone begins to decay. As discussed in the introduction, the processes of cyclone decay or "spin down" have not been as thoroughly studied as those contributing to "spin up" even though the stages of maximum intensity and cyclolysis typically characterize over one half of the cyclone life cycle. However, two processes appear to be important components of cyclolysis: the barotropic transfer of kinetic energy to other scales, and frictional dissipation (Carlson, 1994).

From an energetics perspective (e.g., Smith, 1980), extratropical cyclones grow from the conversion (Figure 2.4) of zonal available potential energy to eddy available

potential energy, and from the conversion of eddy available potential energy to eddy kinetic energy. These baroclinic conversions occur through the advection of warm air poleward and cold air equatorward and through the action of thermally direct (warm air rising, cold air sinking) circulations, respectively. Another potentially important energy transformation that occurs during the life cycle of a cyclone is the conversion of eddy kinetic energy to zonal (or lower wave number) kinetic energy (Figure 2.4). This barotropic conversion is determined by the product of the eddy transport of momentum and the gradient of zonal momentum (Palmen and Newton, 1969) and generally transfers kinetic energy upscale and away from the baroclinic wave. It is relatively small during cyclogenesis but increases as the eddy flow intensifies and the upper waves tilt such that westerly momentum is advected toward the zonal wind maximum (the jet). An example of the variation with time of the baroclinic and barotropic conversions of energy during simulations of idealized baroclinic waves can be found in Simmons and Hoskins (1979). Their results show that up to day eight the baroclinic processes dominate and the energy of the disturbance grows (Figure 2.5). Thereafter, the baroclinic conversions decrease in magnitude while the barotropic conversion from eddy to zonal kinetic energy increases and eventually becomes dominant (Simons, 1972).

The other important cyclolysis mechanism arises owing to friction. Two forms of frictional dissipation have been shown to be important, the dissipation owing to internal friction (Simmons and Hoskins, 1979) and the dissipation owing to boundary layer or surface friction. In the planetary boundary layer (PBL), the balance between the frictional, pressure gradient, and Coriolis forces,

8

$$fk \times \vec{v} - \alpha \vec{\nabla} p + \vec{F} = 0, \qquad (2.1)$$

necessitates a cross-isobaric flow from high to low pressure. This implies a mass convergence (divergence) in cyclonic (anticyclonic) circulations. By mass continuity the convergence in cyclonic flow requires upward vertical motion out of the PBL, which maximizes at the top of the layer. The flux that results from this frictionally induced secondary circulation is often referred to as "boundary layer" or "Ekman" pumping. Holton (1992) shows that the magnitude of the vertical motion is proportional to the geostrophic vorticity.

Although the frictional convergence in the PBL by itself might be thought to spinup vorticity and act as a cyclogenetic agent, it in fact spins down vorticity and contributes to cyclolysis. Qualitatively, the frictionally induced convergence in the boundary layer is compensated for by divergence in the layer above (Carlson, 1994), which results in cyclonic vorticity destruction. Holton (1992) shows that the degradation of geostrophic vorticity owing to the secondary circulation is given by

$$\zeta_g(t) = \zeta_g(0) \exp(-t/\tau_e), \qquad (2.2)$$

where $\zeta_g(0)$ is the geostrophic vorticity at the initial time $t = 0$ and τ_e is the time it takes the initial vorticity to decrease by a factor e^{-1}, i.e., the "e-folding time". He goes on to show that in a barotropic atmosphere the secondary circulation extends throughout the full depth of the vortex, which results in an e-folding time of

$$\tau_e = \left(\frac{2H^2}{fK_m} \right)^{1/2}, \qquad (2.3)$$

9

where H is the height of the tropopause, f is the Coriolis parameter, and K_m is the diffusion coefficient. For typical mid-latitude synoptic scale values, τ_e is on the order of four days, which is significantly larger than the decay time that is due to viscous diffusion of the order one hundred days. In a stably stratified baroclinic atmosphere, buoyancy forces suppress vertical motion and the secondary circulation is restricted to the vicinity of the boundary layer, which tends to reduce the effects of the friction. Carlson (1994) finds a spin-down time on the order of ten days when taking into account the boundary layer depth.

There have been relatively few studies that have directly examined the effects of frictional dissipation on cyclones. In a theoretical study, Farrell (1985) found that the inclusion of Ekman damping severely limits the range of unstable wave numbers as well as the growth rates of the remaining instabilities. Numerical sensitivity studies by Graystone (1962), Danard (1969), and Kuo and Reed (1988) found weaker cyclones in the presence of surface friction. Anthes and Keyser (1979) found that friction increased the minimum central pressure of an extreme case of cyclogenesis over land by almost 20 mb and decreased the PBL winds by a factor of two. The greater frictional convergence resulted in greater rainfall rates, despite a weaker storm intensity.

Significantly, the method by which boundary-layer friction is parameterized may effect the simulation of cyclone life cycles including cyclolysis. The friction terms in the mean-flow horizontal momentum equations are often written in the form:

$$F_x = -\frac{1}{\rho}\frac{\partial(\overline{\rho u' w'})}{\partial z} = \frac{1}{\rho}\frac{\partial \tau_x}{\partial z},$$

and (2.4)

$$F_y = -\frac{1}{\rho}\frac{\partial(\overline{\rho v' w'})}{\partial z} = \frac{1}{\rho}\frac{\partial \tau_y}{\partial z},$$

where the primes represent fluctuating or eddy quantities. In equation (2.4), the covariance terms in parentheses are the eddy fluxes of momentum and are commonly referred to as eddy stresses, which are denoted as τ_x and τ_y. Since in general, the eddy stress distribution is not known, approximations or closure assumptions must be used to relate the stresses to other known quantities. A common method (Haltiner and Williams, 1980) is to assume that the surface stress is parallel to the surface wind and proportional to a drag coefficient C_d such that

$$\vec{\tau} = \rho_s C_d |\vec{V_s}|\vec{V_s} ,$$ (2.5)

where the subscript "s" refers to surface values. The drag coefficient tends to vary with wind speed, static stability, and roughness. It has a value of about 10^{-3} over water, but may be several times that magnitude over land.

One possible source of error in numerical simulations of maritime cyclones is the neglect of wind-wave interactions in the friction parameterization. In particular, under neutral stratification and relatively rough flow

$$C_d(z) = k^2 [\ln(z/z_o)]^{-2} ,$$ (2.6)

where k is the von Karman constant and z_o is the roughness length. Over the open ocean, z_o is typically given by the Charnock formula (Charnock, 1955)

$$z_o = \alpha \frac{\tau}{g\rho} ,$$ (2.7)

11

where α is a constant. Studies by Janssen et al. (1989), Janssen (1991) and Nordeng (1991) suggest that the effect of wind-generated ocean waves can have an important influence upon the wind stress. Ulbrich et al. (1993) found that increased surface roughness in the Southern Hemisphere storm track significantly modified the tropospheric circulation. Doyle (1995) performed high resolution numerical experiments with a constant surface roughness, a roughness length from Charnock's formula, and a roughness length obtained from a coupled ocean-wave/atmosphere mesoscale model. The parameterization method used to couple the wave-atmosphere models incorporates the effects of a mixed sea with

$$z_o = \beta \frac{\tau}{g\rho(1 - \tau_w / \tau)^{1/2}}, \qquad (2.8)$$

where τ is the total stress, τ_w is the wave-induced stress, and β is a constant. Doyle found that young ocean waves increased the effective roughness up to a factor of 5, changed the drag coefficient up to 50%, increased the surface stress, and significantly decreased the low-level wind speeds. Moreover, although the frictional changes owing to ocean waves are complex, they appear to modulate the deepening rate during cyclogenesis and for the purposes of this thesis augment the cyclone filling process.
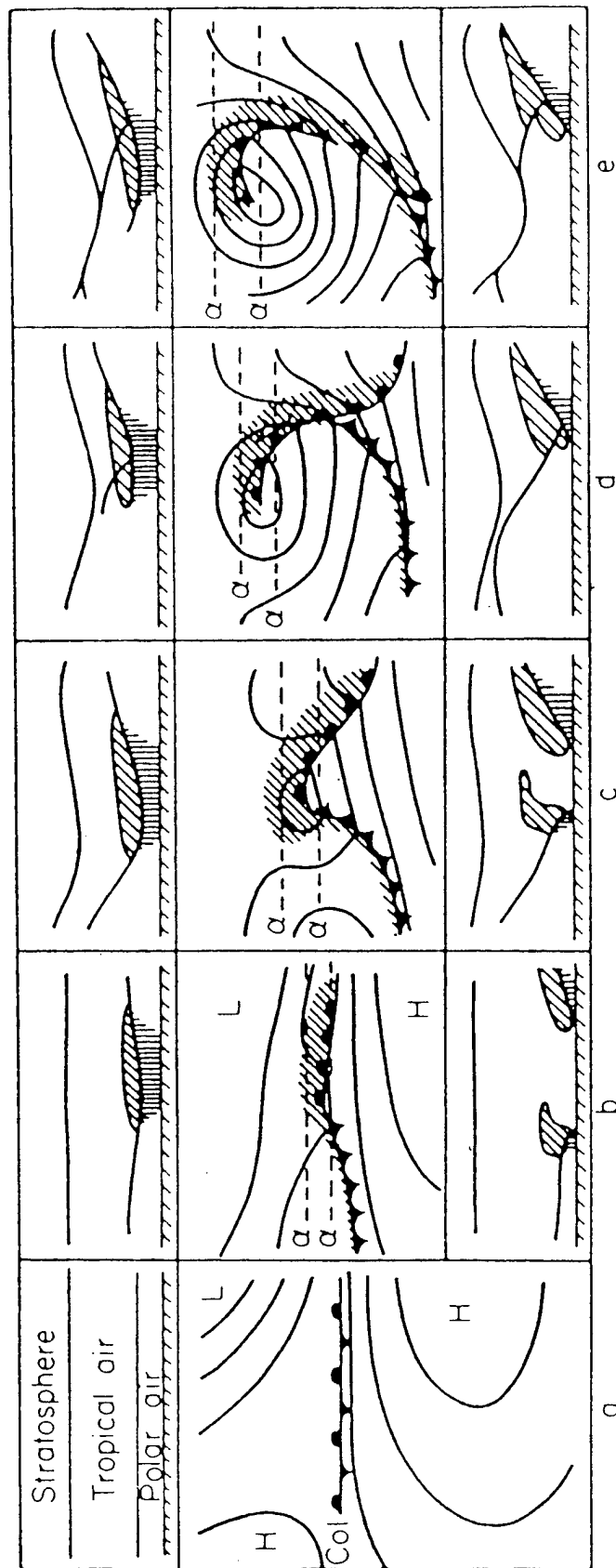
Figure 2.1. Schematic of the Norwegian extratropical cyclone life cycle from genesis (b) to dissipation (e). In middle figures, thin lines are sea-level isobars, and fronts are depicted with half triangles and circles. Top and bottom figures show schematic clouds, frontal surfaces, and tropopause along lines α, just north and south of cyclone center. The times between stages (a) and (c), and between stages (c) and (e), correspond approximately to one day in each case. (Palmen and Newton, 1969)
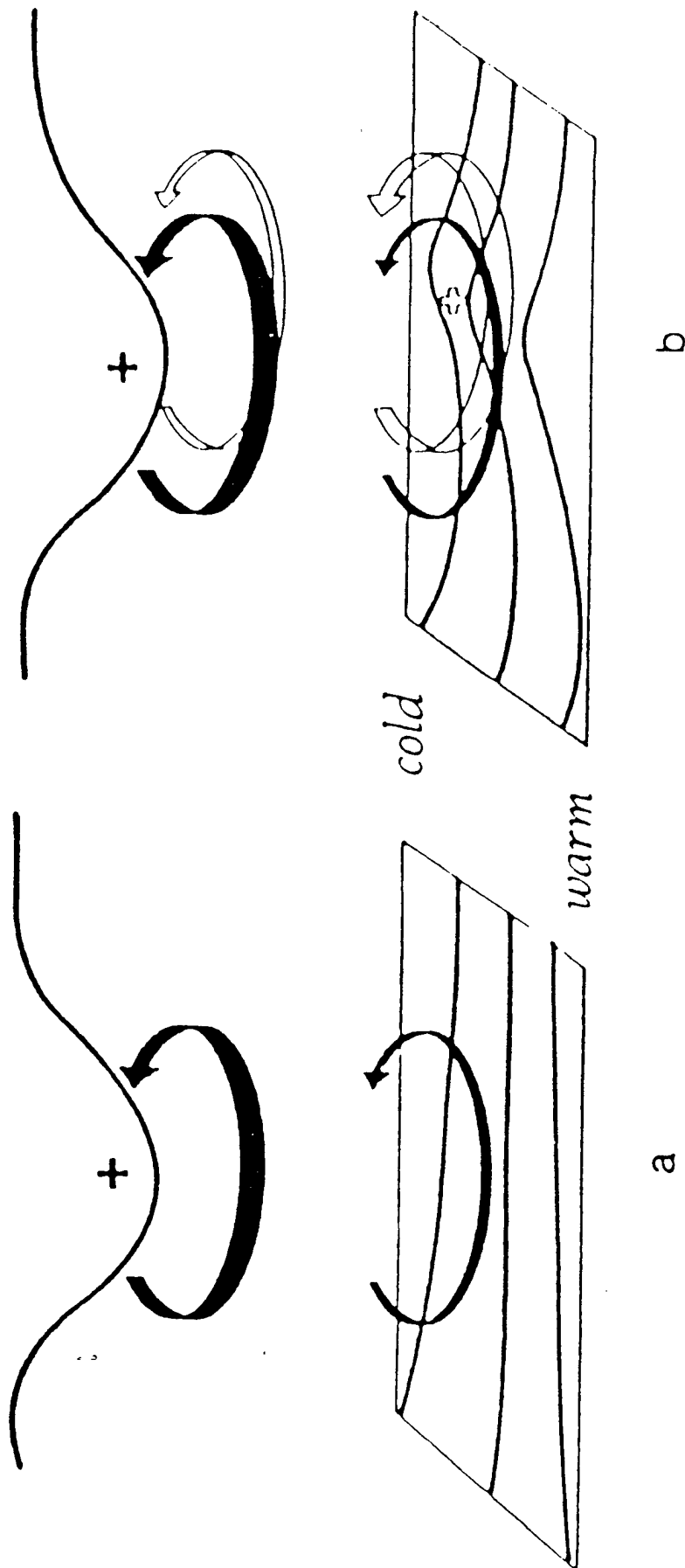
Figure 2.2. A schematic of cyclogenesis associated with the arrival of an upper-air potential vorticity anomaly over a low-level baroclinic region. In (a), the upper-air cyclonic potential vorticity anomaly, indicated by a solid plus sign and associated with the low tropopause shown, has just arrived over a region of significant low-level baroclinicity. The circulation induced by the anomaly is indicated by solid arrows, and potential temperature contours are shown on the ground. The low-level circulation is shown above the ground for clarity. The advection by the circulation leads to a warm temperature anomaly somewhat ahead of the upper potential vorticity anomaly as indicated in (b), and marked with an open plus sign. This warm anomaly induces the cyclonic circulation indicated by the open arrows in (b). (Hoskins et al., 1985)
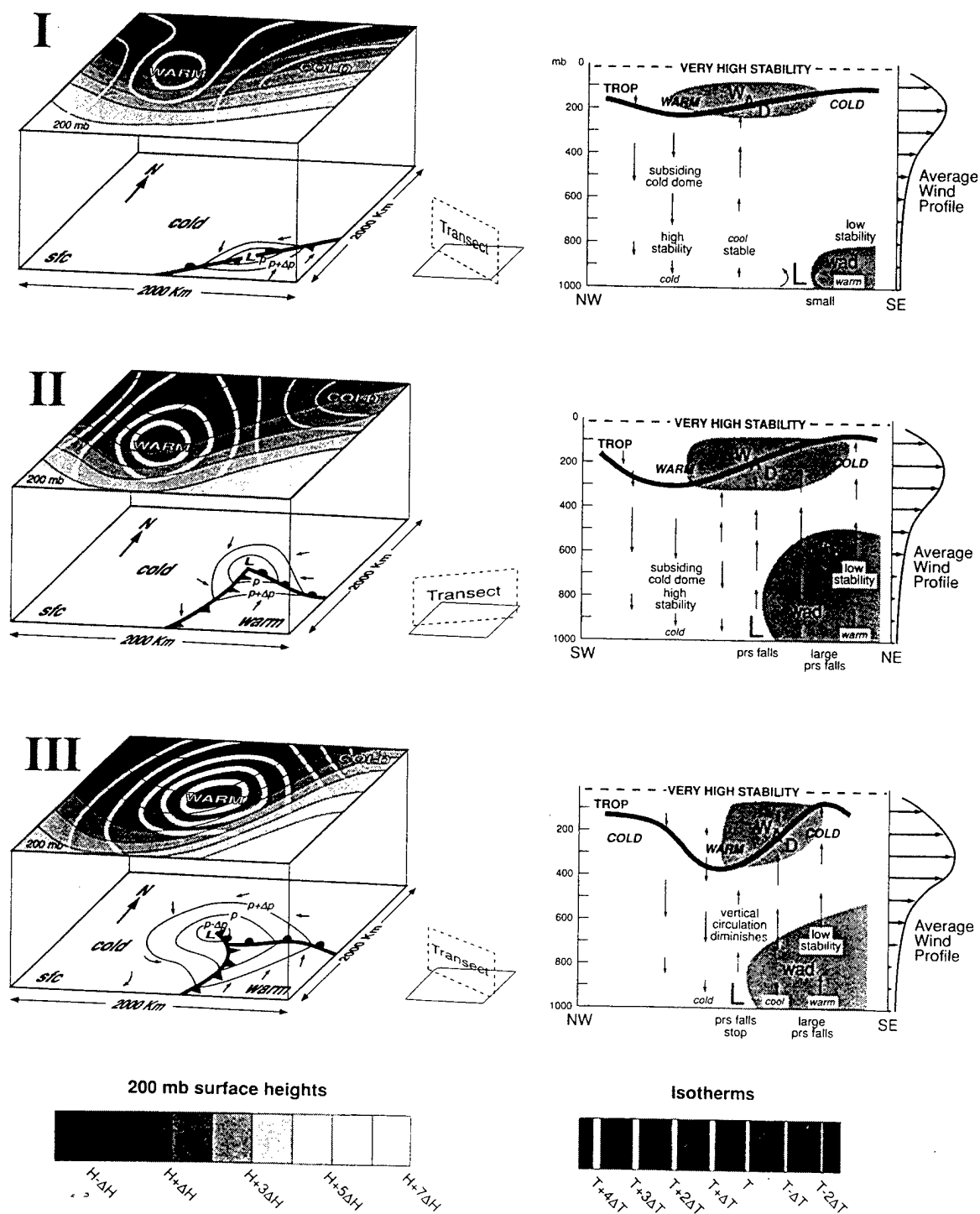
14

Figure 2.3. Schematic of the evolution of the temperature advection and vertical motion patterns associated with a developing tropopause undulation and surface cyclone from cyclone inception (I), to most rapid deepening (II), to maximum intensity (III). (Hirschberg and Fritsch, 1991b)
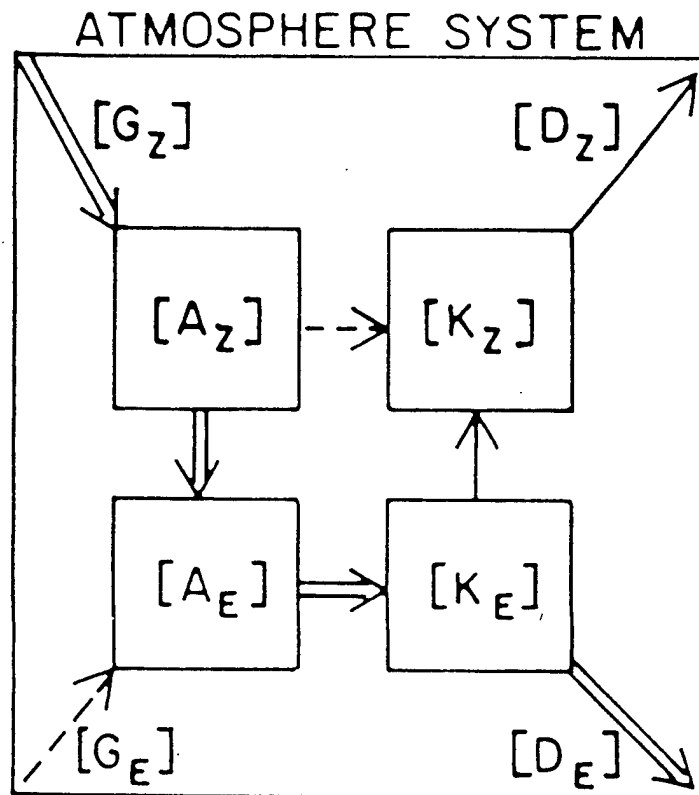
15

Figure 2.4. Schematic energy and energy conversion diagram of the atmospheric system. Bracketed symbols within the boxes refer to mean zonal (Z) and eddy (E) components for kinetic energy [K] and available potential energy [A]. Energy inputs in the form of diabatic heating [G] and frictional dissipation [D] are shown. Arrows denote the most likely direction of the conversion between energy components for a large-scale mid-latitude region averaged over the passage of many disturbances. Bold-faced arrows denote a generally large rate of conversion, thin arrows a small rate of conversion and broken arrows a very small rate of conversion or one that is not consistently in one direction. (Carlson, 1994)
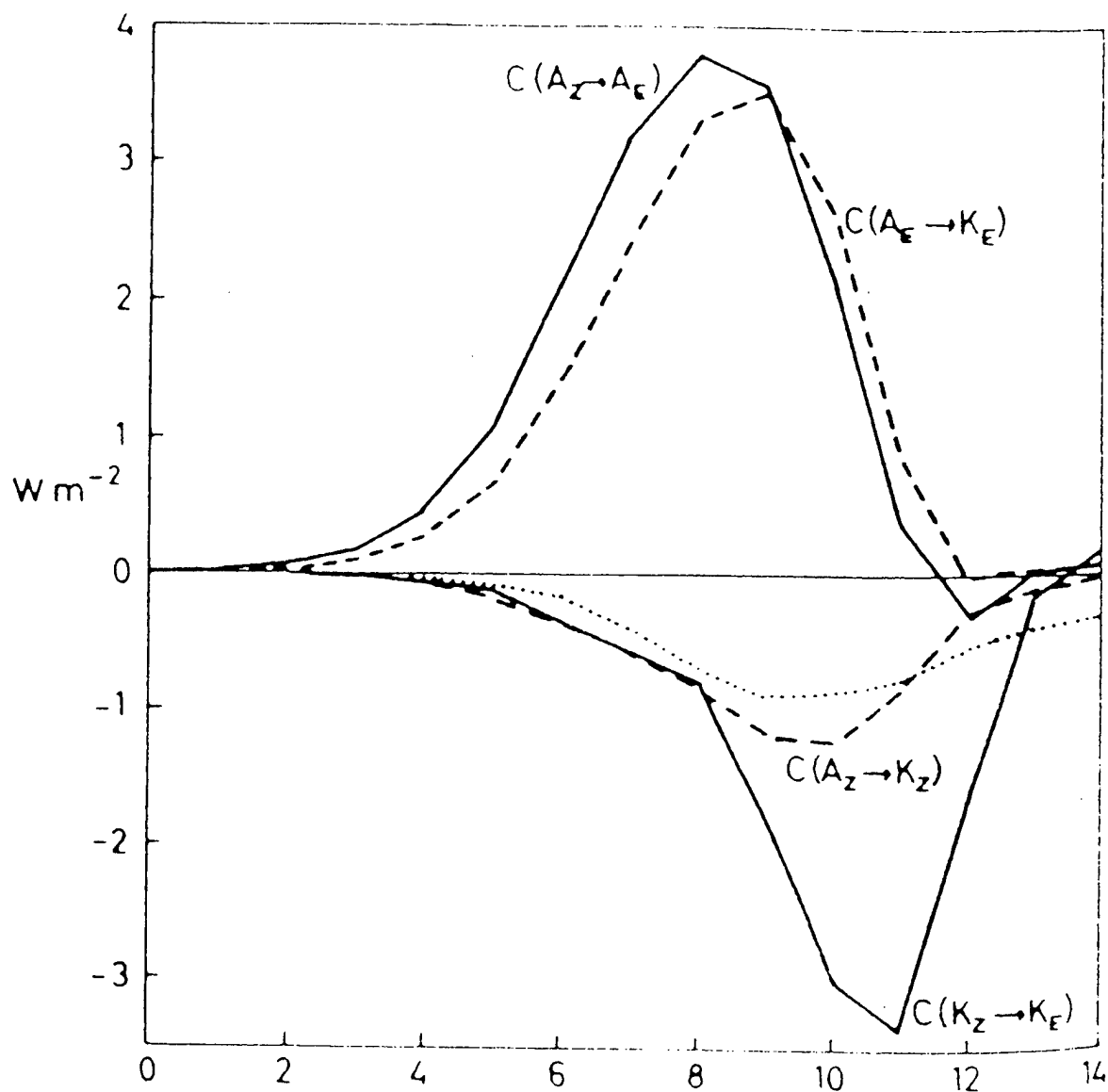
Figure 2.5. Variation with time of various energy conversions and the net rate of energy dissipation (dotted curve) in a numerical simulation of an idealized baroclinic wave. Symbols A_Z and A_E are the zonal and eddy available potential energies, and KZ and KE the corresponding kinetic energies. Positive values of $C(A_Z => A_E)$ imply a baroclinic transfer from A_Z to A_E, and negative values imply a barotropic transfer. (Simmons and Hoskins, 1979).

17

III. DATA AND METHODOLOGY

Two different types of data sets were used to study the decay characteristics of analyzed and predicted extratropical cyclones over the North Pacific Ocean. Specific features associated with various sea-level pressure cyclones were defined from a data base that is produced operationally by Fleet Numerical Meteorology and Oceanography Center (FNMOC). Characteristics of the large-scale synoptic flow over the North Pacific Ocean were defined from fields produced by the Navy Operational Global Atmospheric Prediction System (NOGAPS).

This study concentrates on cyclones that occurred during the autumn (i.e., October - December) and winter (January - March) seasons. The period of study, which begins in January 1994 and ends in February 1996, was chosen to coincide with the operational use of NOGAPS Version 3.4. NOGAPS is a global spectral numerical weather prediction model that contains data quality control, data assimilation, nonlinear normal mode initialization and a sophisticated suite of physical parameterizations (Hogan and Rosmond, 1991). Version 3.4 operates at a spectral resolution of 159 waves with 18 vertical levels that extend to 10 mb. The vertical coordinate is a hybrid system that follows the terrain at low levels and constant pressure surfaces at upper levels.

A. SEA-LEVEL PRESSURE CYCLONE DATA

On an operational basis, forecast verification statistics that pertain to sea-level pressure cyclones are produced at FNMOC. These statistics are computed from physically relevant parameters that are defined by tracking individual cyclones (Harr et al., 1992) that exist in the NOGAPS 0000 UTC and 1200 UTC daily analysis and forecast

sea-level pressure fields. A cyclone is defined in the analysis or forecast field by the presence of at least one closed isobar. Each cyclone is given a unique identifier and various physical features such as location and central pressure are stored in a large data base. When an existing cyclone is no longer identifiable by a closed isobar in the analyzed sea-level pressure field, the cyclone is finalized and all data that pertain to the life of the cyclone are archived. The archived data are then used to define various forecast error statistics.

The archived data base of sea-level pressure cyclone characteristics were used to define the physically relevant parameters needed to study the filling characteristics of cyclones over the North Pacific Ocean. The deepening and filling stages of each cyclone were defined by the analyzed central pressures. Deepening (filling) was defined as a central pressure decrease (increase) over a 12-h period. To be included for study, a cyclone must have existed for a minimum of 36 hours, deepened for a minimum of 12 hours to a minimum central pressure, and then filled for a minimum of 24 hours after maximum intensity. Because cyclones at different latitudes with identical pressure gradients do not produce the same maximum geostrophic winds, all central pressures were normalized to a latitude of 42.5° north. This was necessary because storms at different latitudes with identical pressure gradients do not produce the same maximum geostrophic wind. Using 42.5° as the reference latitude, the normalization technique for pressure differences is $\Delta P_n = \Delta P (\sin 42.5°/\sin \phi)$ where ϕ is the latitude of the pressure comparison (Roebber, 1984).

Sea-level pressure cyclone characteristics at the time of maximum intensity, maximum filling, and storm end were used to define various attributes of the filling

cyclones. A homogenous sample was insured by only choosing cases where data were defined for all three stages of the filling life cycle.

Forecast central-pressure errors and position errors were computed by subtracting the verifying analysis value from the forecast value. A negative (positive) central-pressure error corresponds to a forecast pressure that is lower (higher) than the analyzed value and is labeled as overforecast (underforecast). The forecast position error was defined as the absolute distance (km) between the forecast and verifying analysis positions.

B. SYNOPTIC-SCALE FIELD DATA

One goal of this study is to identify aspects of filling cyclones with synoptic-scale features over the North Pacific Ocean. Relevant synoptic features that are associated with each cyclone obtained from the sea-level pressure cyclone data base were identified from fields obtained from the NOGAPS analysis and forecast fields. The field data were obtained on a 2.5° latitude/longitude grid, which corresponds to the standard output products produced at FNMOC. Sea-level pressure fields were converted to departures from a zonal mean. The zonal mean was removed under the assumption that a cyclone will be limited to fill up to the background pressure field at the respective latitude. An example of a sea-level pressure field that has been converted to departures from the zonal mean is provided in Figure 3.1.

In addition to the filling characteristics that can be defined from the sea-level pressure cyclone data base, other operationally and physically important parameters were identified. These include the change in size of the cyclone as it fills and the change in the size of the area enclosed by winds of gale force or stronger. The size of a cyclone is defined by the area (km^2) enclosed by the outer closed isobar in the analyzed and forecast

sea-level pressure field after the zonal means have been removed. Similarly, the size of the gale area is computed as the area containing wind speeds greater than 15 m s^{-1}. To compute these areas, the sea-level pressure field was interpolated to a cylindrical grid that was placed at the center of each cyclone. The cylindrical grid has a radius of 10 degrees of latitude and data were interpolated to a 1 degree latitude spacing (Figure 3.2).

Several other characteristics of the filling extratropical cyclones were computed from the combination of data from the sea-level pressure cyclone data base and the NOGAPS field data. Each parameter was defined for the NOGAPS analysis and 48-hour forecast fields. The rate of filling is defined in terms of an e-folding time (τ_e) given by

$$\tau_e = \{(dP/dt)/D\}^{-1} \tag{3.1}$$

where P is the cyclone central pressure as defined in the cyclone data base and D is the sea-level departure from the zonal mean.

The average wind inside the outer closed sea-level pressure isobar is defined at 1000 mb and 925 mb. Agradient winds are computed as a difference between the gradient wind that is computed on the cylindrical grid and subtracted from the winds defined in the NOGAPS fields. An average agradient wind inside the outer closed isobar is used as an estimate of frictional influence at low levels.

The barotropic conversion of eddy kinetic energy to zonal kinetic energy (K_Z to K_E) is computed at 300 mb as:

$$B_C = \overline{u'v'} \, (\partial u/\partial y) \tag{3.2}$$

where u is the zonal wind, v is the meridional wind, and primed values represent a departure from a zonal mean that is represented by the overbar.

While combining the two data sets, approximately 50% of the field data did not match with the cyclone data storms. There are several reasons for this. First, there were several months of field data that were not available. Second, several data fields were not available for different time periods. Lastly, some of the data was contaminated or not saved properly.

In summary, by matching the sea-level pressure cyclone data with the synoptic-scale field data, several characteristics of filling extratropical cyclones were computed. These attributes are based on features of the cyclone itself and on the synoptic-scale flow over the cyclone region. Most comparisons will be made at three points in the life cycle of the filling cycle. These are defined as the time that the cyclone is at maximum intensity, the time of maximum filling, which is defined by the maximum 12-h change in central pressure, and the last time that the cyclone is identified with an outer closed isobar. All parameters are computed from the NOGAPS analysis and 48-h forecast fields.
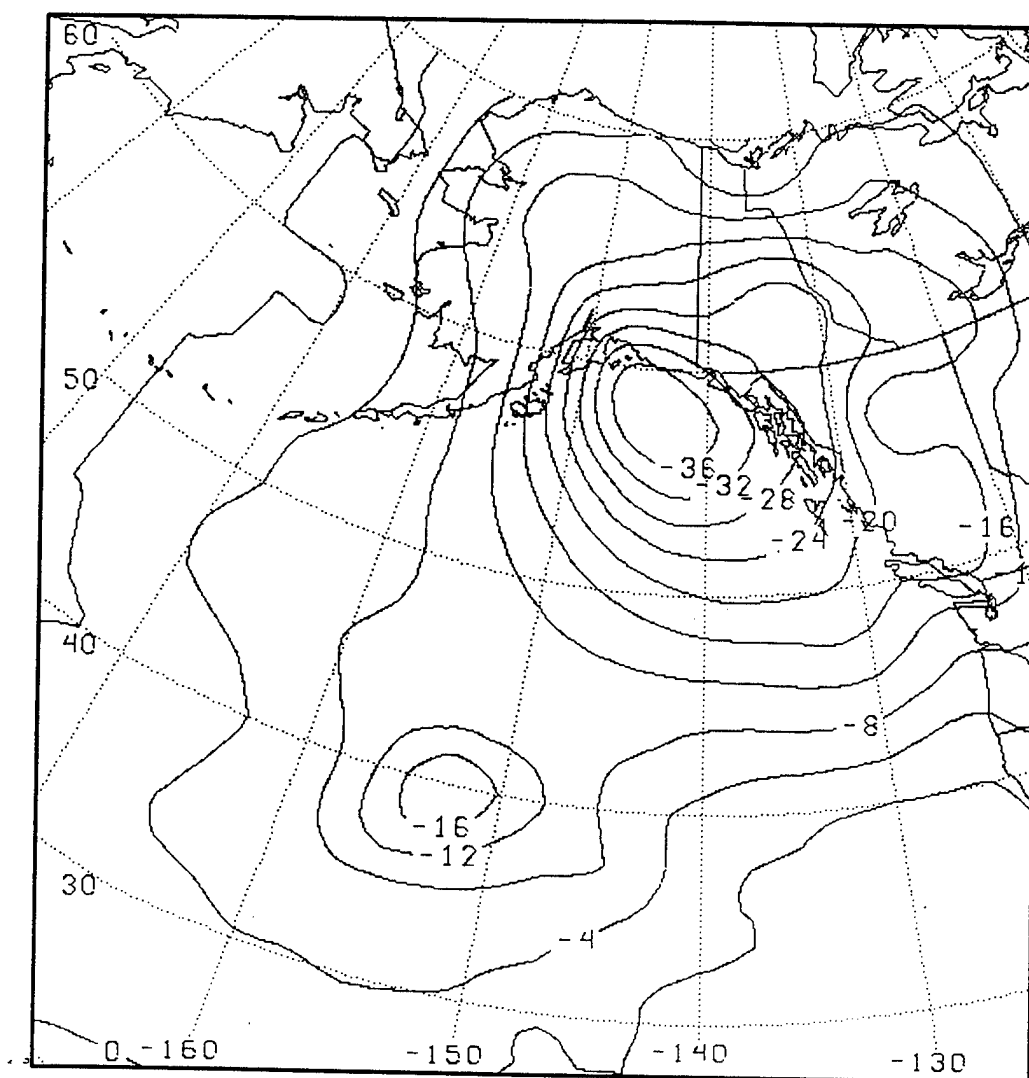
Figure 3.1. An example of a sea level D-value pressure field (mb). The D-value is the departure from the zonal mean (SLP-ZM).

Area enclosed by outer closed isobar

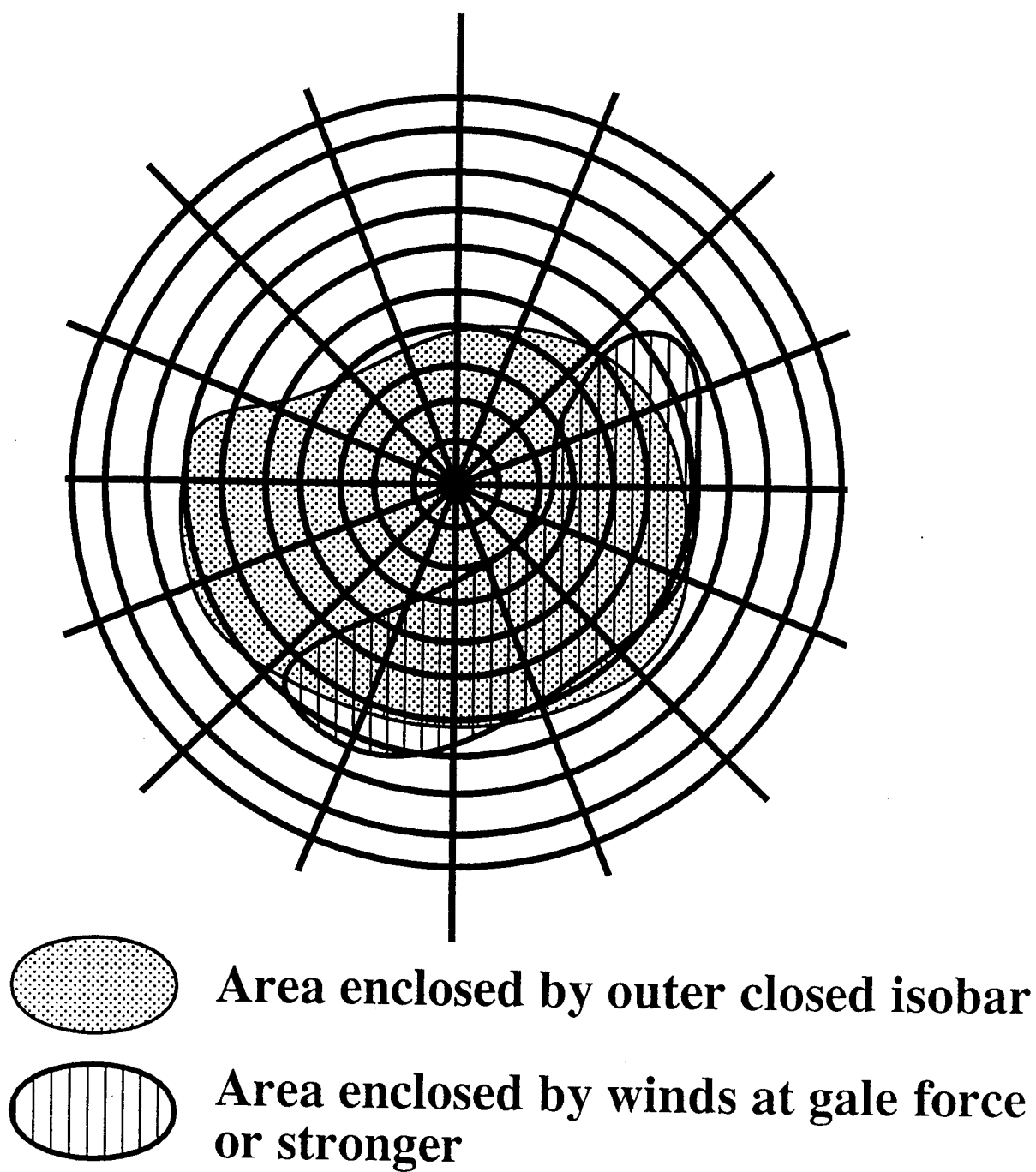**Area enclosed by winds at gale force or stronger**

Figure 3.2. The 1° latitude cylindrical grid utilized for field data calculations. The radius of the grid is 10° latitude and the surface low is located at the center. Example cyclone and gale areas are stipled and hatched, respectively.

IV. RESULTS

A total of 98 NOGAPS analysis Pacific cold-season storms in the study period met the criteria defined in Chapter III. Of these 98, 60 analyzed storms had matches in the set of 48-h forecasts. There are two portions of data analysis. First, the cyclolysis characteristics in the NOGAPS analysis for five track types over the North Pacific are examined. Second, the 48-h forecast cyclolysis characteristics are examined to determine if any systematic model differences are present.

For all analysis and 48-h forecast storms, the sea-level cyclone data from FNMOC provided date, time, and position of storm genesis, maximum deepening, maximum intensity, maximum filling, and storm dissipation. From this information, frequency distributions of the above parameters were produced (Figure 4.1) by normalizing the number of events in 5° latitude by 5° longitude boxes over the study period to 42.5°. In addition, average/maximum deepening rates, maximum intensity central pressures, average/maximum filling rates, average filling translational speeds, and filling translational distances were calculated using the sea-level cyclone data.

A. ANALYSIS CHARACTERISTICS

It is evident from Figure 4.1, that there are three primary regions of cyclone activity. Cyclones that form in the western Pacific, typically develop near the Kuroshio current and either move meridionally into the Sea of Okhotsk or move zonally over the central Pacific. Cyclones that form in the central Pacific, either curve northward to an area just east of the Kamchatka Peninsula or move eastward into the Gulf of Alaska. Secondary cyclones often develop in the eastern Pacific and then dissipate in the Gulf of

Alaska. In general, these distributions closely correspond to those defined by Petterssen (1956), Zishka and Smith (1980), Gyakum et al. (1989), and Harr et al. (1992). Not surprisingly, many migrating storms dissipate in the well-known cyclolysis regions near the Kamchatka peninsula and the Gulf of Alaska where deep semi-permanent lows reside. Average deepening and filling rates (Figure 4.2) for the sea-level cyclones used in this study are -6.33 mb/12-h and 4.19 mb/12-h. Gyakum (1983) defined an explosively deepening cyclone (a bomb) as one that deepens 24 mb in 24 hours at 45° latitude. Examination of the filling rates in Figure 4.2 reveals that there are also several instances of explosive filling cyclones (anti-bombs) that fill at a commensurate rate of 12 mb in 12 hours.

To isolate analysis filling characteristics, the tracks from maximum intensity to storm dissipation were developed for each cyclone. These tracks were then separated into five different categories (Figure 4.3) based on inferred synoptic-scale flow patterns. The five category types consist of: 1) western Pacific (west of 180°) storms that dissipate in the primary low located in the Sea of Okhotsk, 2) western Pacific storms that move northward and dissipate east of the Kamchatka Peninsula, 3) central Pacific storms that move zonally and dissipate in the Gulf of Alaska, 4) eastern Pacific (east of 180°) storms that curve and dissipate in the Gulf of Alaska, and 5) storms that originate and dissipate in the open ocean. The statistical significance of track type one was concluded to be questionable owing to the low number of storms in the category (Figure 4.3). Therefore, results based on Type one will not be discussed.

Field data values for storms with matching NOGAPS analyses were determined for the following parameters: D-value, gale area, cyclone area, cyclone equivalent radius,

28

500-mb geopotential height low and 200-mb temperature maximum offsets from the surface low position, and 1000-mb and 925-mb gradient winds (V_G), agradient winds (V_{AG}), and observed winds (V). According to the modern conceptualization of cyclogenesis (see Chapter II), storms stop deepening when the upper-level dynamics have moved downstream of the surface low center and the upper-level trough is located directly over it. The 500-mb low offsets (Figure 4.4) at the time of maximum surface low intensity for each of the track types are consistent with this model. A case for the claim by Hirschberg and Fritsch (1991 a,b) that occlusion occurs when the 200-mb warm pool is over the surface low can be made with the 200-mb temperature offsets (Figure 4.5), although there is a large amount of variability in the small sample.

A comparison of filling characteristics according to track type reveals a systematic pattern of differences between track categories two and four and categories three and five. This might have been expected since Types two and four move meridionally and dissipate in areas of semi-permanent, primary low pressure systems, while Types three and five are fast, zonally moving systems. In particular, Types three and five move much faster and farther than two and four (Figure 4.6 and Figure 4.7). While Type two and four storms have larger D-values from maximum intensity to maximum fill, the tend to be slightly smaller than Type three and five storms (Table 4.1).

One of the more important characteristics examined was filling rate. Rather than using the pressure tendency to judge filling, we chose to evaluate an e-folding rate parameter (τ_e) defined as the pressure tendency at the cyclone center divided by the cyclone D-value at maximum intensity (Equation 3.1). Looking at the filling rates in terms of τ_e has the benefit of normalizing deep versus weak storms and also enables a

comparison of our results with the theory of frictional decay. Examination of Table 4.1 and figure 4.8 shows that Type three and five storms tend to fill faster than Types two and four storms. In particular, Types three and five decay at a rate that is one day faster than Types two and four. This result, in addition to the finding that Types three and five storms move faster, is consistent with Doyle's (1995) hypothesis that faster moving maritime cyclones decay more quickly due to increased wind-new wave interaction. The faster decay rates for Types three and five are also consistent with the larger 1000-mb and 925-mb agradient winds (V_{AG}) found in this category (Table 4.1).

There has been some speculation (Simmons and Hoskins, 1979) that storms fill at about the same rate as they deepen. The analyzed average deepening rate/fill rate ratios (Figure 4.9) found in this study contradicts this hypothesis. All five track types had average ratios greater than one indicating that the average deepening rates were greater than the average filling rates. The ratio of maximum deepening/filling rate was also greater than one for all track types (Table 4.1).

Of high interest to forecasters concerned with maritime cyclones is the extent of gale area associated with the mature cyclone and how the gale area size changes as the cyclone decays. Previous studies have not considered gale area characteristics during cyclone evolutions. Not surprisingly, we find that the largest absolute gale areas, as well as the ratio of gale area to cyclone size occurs at cyclone maximum intensity (Table 4.1). Although Type five storms have the largest gale areas, there are no discernible trends between categories. Of note, however, are the changes in gale area from cyclone maximum intensity to the end of the storm (Figure 4.10). Once again, there are major differences between Types two and four and Types three and five. Gale area changes for

30

Types three and five are less variable than Types two and four. We postulate that this is due to the fact that Type three and five storms consist of lows that form distinctive gale area patterns in the open ocean, while Types two and four are complex lows in the primary cyclolysis regions.

Finally, we examine whether the barotropic energy conversion and surface drag mechanisms of cyclone decay that were discussed in Chapter II, are evident in the NOGAPS analysis fields. Figure 4.11 shows boxplots of the barotropic conversion term B_C in Equation (3.2). All five categories show the conversion to be positive, which means that eddy kinetic energy of the storms is being converted to zonal kinetic energy. However, the importance of this decay mechanism can not be determined.

A drag coefficient is often used to parameterize the effects of friction. In particular, Carlson (1994) shows that the e-folding decay time τ_{ef} owing to friction is given by

$$\tau_{ef} = \Delta P_f / (g \, \rho_s \, C_D \, |V_s|), \tag{4.1}$$

where ρ_s is surface density, $|V_s|$ is surface wind speed, ΔP_f is the depth of the friction later (PBL), and C_D is the drag coefficient. Theory (Stull, 1988) and observations (Figure 4.12) show that C_D increases with wind speed in a more-or-less linear fashion. Therefore, the cyclone decay rate should increase with increasing wind speed if friction is operating and assuming that ρ_s and ΔP_f are constant. The average observed 1000 mb and 925 mb wind speeds and e-folding decay rates, τ_e, found for the five track types (Table 4.1) are qualitatively consistent with these previous results. Storms in Types three and five have larger average winds (until storm end) and smaller τ_e's then Type two and four storms.

STORM CATEGORY	AVG E-FOLDING (days)					MAX E-FOLDING (days)				
	1	2	3	4	5	1	2	3	4	5
MEANS	4.76	6.55		5.78	4.39	3.34	5.01		3.51	3.26

STORM CATEGORY	GALE AREA(*1000km²)					1000 mb FRICTION(Vag - m/s)				
	1	2	3	4	5	1	2	3	4	5
MAX INTENSITY	1141	1832	1822	1340		-13.80	-14.61		-13.59	-15.47
MAX FILL	1403	1510	1357	923		-12.48	-12.25	-12.35	-10.58	
STORM END	552	1070	576	312		-8.72		-6.33	-5.62	-5.97
FILL - INTENSITY	54	-322	-465	-530		1.32	2.36		2.96	0.97
END - INTENSITY	-534	-844	-1177		-1253	5.08	6.16		7.86	9.50
END - FILL	325	-636	-725		-614	3.76	3.80	6.03	4.96	

STORM CATEGORY	FILL SPEED (m/s)					FILL DISTANCE (KM)				
	1	2	3	4	5	1	2	3	4	5
MEANS	3.52	4.73	7.76	3.75		507	719		640	1419

STORM CATEGORY	D-VALUE (mb)					GALE AREA/SIZE RATIO				
	1	2	3	4	5	1	2	3	4	5
MAX INTENSITY	-35.5		-34.4	-36.2	-32.8	0.516	0.899	0.832	0.769	
MAX FILL	-31.5		-28.1	-31.6	-30.2	0.656		0.722	0.511	0.610
STORM END	-18.2		-16.5	-20.3	-22.6	0.309	0.664	0.433	0.399	
FILL - INTENSITY	3.92	4.91		4.56	2.57	0.045	-0.132	-0.110		-0.306
END - INTENSITY	17.23	12.45		15.89	10.13	-0.208	-0.298	-0.418		0.072
END - FILL	13.32	7.54		11.33	7.57	-0.212	-0.219	-0.350	-0.193	

STORM CATEGORY	Avg. Deep/Fill rate ratio (mb/12 hrs)					Max Deep/Fill rate ratio (mb/12 hrs)				
	1	2	3	4	5	1	2	3	4	5
MEANS	1.50	2.38	1.84	0.19		1.50	3.13		1.91	1.67

STORM CATEGORY	Size - Eqv Radius (deg lat)					925 mb FRICTION(Vag - m/s)				
	1	2	3	4	5	1	2	3	4	5
MAX INTENSITY	7.52	7.45	7.59	7.11		-13.36	-14.10		-13.02	-15.07
MAX FILL	7.00	7.39	7.24	6.81		-11.38	-11.88	-11.65	-9.94	
STORM END	6.08		4.88	5.56	4.57	-7.64		-5.93	-5.00	-5.90
FILL - INTENSITY	-0.52	-0.06		-0.29	-0.23	1.98	2.22		3.09	1.13
END - INTENSITY	-1.43	-0.58	-2.71	-1.54		5.72	6.56		7.95	9.17
END - FILL	-0.92	-0.52	-2.36	-1.25		3.74	4.09	5.72	4.86	

STORM CATEGORY	1000 mb OBSERVED WINDS(V - m/s)					925 mb OBSERVED WINDS(V - m/s)				
	1	2	3	4	5	1	2	3	4	5
MAX INTENSITY	11.94	14.07		12.59	15.07	14.28	16.91	18.94	15.16	
MAX FILL	12.58	12.49	12.25	10.19		14.00	15.08	14.68	11.79	
STORM END	9.10	10.09	7.85	7.51	8.07	9.86		8.74	8.07	9.37
FILL - INTENSITY	0.64	-1.58		-2.39	-1.87	-0.28	-1.83		-3.37	-2.20
END - INTENSITY	-2.84	-3.98		-5.13	-7.00	-4.42	-5.69		-7.14	-9.63
END - FILL	-3.48	-2.40	-4.40	-2.68		-4.14	-3.66	-5.94	-3.76	

Table 4.1. NOGAPS analysis characteristic means for the five track types based on 98 total extratropical cyclones. Dark shaded boxes highlight the largest track value for each parameter. Lightly shaded boxes highlight the second largest track type.

Of course, the actual decay rate of a cyclone may be dependent on other factors beside friction. Schematically, the actual e-folding decay rate can be expressed as

$$\tau_e = \tau_{ef}(\text{friction}) + \tau_{eb}(\text{barotropic conversion}) + \tau_{eso}\{\text{other sources}\} + \tau_{esi}\{\text{sinks}\}. \quad (4.2)$$

To more quantitatively assess the cyclolytic effects of friction on the storms in our sample, we examined the relationship between storm average e-folding decay rate, wind velocity and drag coefficient. Our goal was to determine whether frictional drag can account for the decay rates we observed. The premise is that if friction is a major influence on the storm e-folding rates then a relationship between C_D and $|V_s|$ similar to that in Figure 4.12 should be present in the data. To examine this relationship the following "synoptic-scale" expression for C_D was utilized

$$C_D = (\Delta P_f) / (g\, \rho_s\, \tau_e\, |V|), \tag{4.3}$$

where τ_e is the average e-folding decay rate, $|V|$ is the average 1000 mb or 925 mb velocity for each storm and the ratio $\rho_s / \Delta P_f$ is considered a constant on the order of 10^{-5}.

Rather than finding that C_D increases with wind speed at a more rapid rate than observed over calm water (Figure 4.12), which would be expected if wind-wave influences were active (Doyle, 1995), we find that the parameterized C_D from model analyzed winds decrease with wind speed (Figure 4.13) at a high degree of significance. This suggests that the observed e-folding rates of these cyclones do not decrease as rapidly as does the observed winds, which further suggests that other mechanisms are reducing the frictional effect.

B. 48-h FORECAST ERROR RESULTS

The next portion of our study involved the statistical comparison of the 60 storms that had matching analysis and 48-h forecasts and also met the selection criteria outlined in Chapter III. The 60 forecast storms were placed in one of the five aforementioned track categories (Figure 4.14) based on the corresponding analysis tracks. The frequency distribution of the 48-h forecast storms are shown in Figure 4.15. These distributions,

33

which were constructed from a smaller sample of storms than the analysis, generally show the same patterns as the analysis distributions in Figure 4.1. The forecast maximum deepening and filling rate histograms in Figure 4.2 are similar to the analysis although there is a paucity of forecast weakly filling storms (Figure 4.16), which is unexplained.

Table 4.2 lists the mean forecast errors associated with the cyclolysis characteristics for each track type. The forecast errors were calculated by subtracting the analysis parameter from the 48-h forecast parameter. As indicated in the analysis results, there are some notable differences between Types two and four and Types three and five. Recall, Type two and four storms are relatively stationary, primary lows, and Type three and five storms are fast moving, open ocean lows. According to FNMOC Performance Summary (FNMOC, 1996), NOGAPS forecasts of large, primary lows that move meridionally are more accurate than faster lows that move zonally. This is apparent in the cyclolysis error statistics (Table 4.2) that show longer fill distance (Figure 4.17) and greater fill speed (Figure 4.18) error for Types three and five storms compared to Types two and four storms. In addition, Figure 4.17 and Figure 4.18 show more variability in the errors associated with Type two and four storms. We believe this is also due to the fact that Type two and four storms can be complex and variable systems that are part of the semi-permanent lows near the Kamchatka Peninsula and the Gulf of Alaska. Of operational interest are the gale area forecast errors (Figure 4.19). Although there are no distinctive forecast model tendencies, there is a large amount of variability between storm categories.

Perhaps surprisingly, in light of wind-wave interaction theory (Doyle, 1995), there is no evidence for any systematic under-prediction of cyclolysis in the 48-h NOGAPS

model over the North Pacific. The D-value errors from maximum intensity to storm end (Table 4.2) are small across all track types. Moreover, ignoring storm Type one results, which are based on only two storms, the model over-predicts the filling of storms (Table 4.2 and Figure 4.20). For example, the average e-folding decay rate for type four storms is 0.94 days faster in the 48-h forecasts.

STORM CATEGORY	AVG E-FOLDING (days)					MAX E-FOLDING (days)				
	1	2	3	4	5	1	2	3	4	5
MEANS	▓	-0.81	-0.36	-0.94	-1.45	-0.01	-0.84	-0.09	0.15	▓

STORM CATEGORY	GALE AREA(*1000km²)					1000 mb FRICTION(Vag - m/s)				
	1	2	3	4	5	1	2	3	4	5
MAX INTENSITY	-697	▓	85	-369	-1256	-0.70	▓	0.37	0.14	1.20
MAX FILL	-426	▓	-42	-51	-564	1.05	0.78	▓	0.08	2.20
STORM END	-1118	▓	206	12	-103	1.25	1.13	▓	-0.20	-0.50

STORM CATEGORY	FILL SPEED (m/s)					FILL DISTANCE (KM)				
	1	2	3	4	5	1	2	3	4	5
MEANS	0.17	-0.46	-1.04	0.08	▓	46.47	-98.36	▓	-83.5	▓

STORM CATEGORY	D-VALUE (mb)					GALE AREA/SIZE RATIO				
	1	2	3	4	5	1	2	3	4	5
MAX INTENSITY	0.45	-3.95	▓	0.02	-0.10	-0.235	▓	0.030	▓	-0.628
MAX FILL	6.10	1.23	-1.13	▓	0.05	-0.091	▓	0.205	0.057	-0.197
STORM END	-1.20	1.85	0.06	▓	-4.10	-0.422	0.151	▓	0.006	-0.623

STORM CATEGORY	Size - Eqv. Radius (deg lat)					925 mb FRICTION(Vag - m/s)				
	1	2	3	4	5	1	2	3	4	5
MAX INTENSITY	-0.35	▓	-0.37	0.35	0.15	-0.15	▓	0.57	0.26	0.80
MAX FILL	-0.30	0.38	-0.60	▓	0.00	0.80	1.28	▓	0.08	1.95
STORM END	-1.90	-0.58	▓	0.43	2.10	0.75	▓	-1.39	-0.23	-0.35

STORM CATEGORY	Mean Barotropic Conversion					Avg. deep rate/fill rate (mb/12hrs)				
	1	2	3	4	5	1	2	3	4	5
MEANS	-1.475	▓	0.193	-0.040	0.125	-0.239	0.113	0.312	▓	0.154

STORM CATEGORY	1000 mb winds (V - m/s)					925 mb winds (V - m/s)				
	1	2	3	4	5	1	2	3	4	5
MAX INTENSITY	1.85	▓	0.63	-0.40	-1.70	2.30	▓	-0.36	-0.44	-1.85
MAX FILL	-0.75	▓	-0.36	-0.30	-2.35	-0.10	▓	-0.54	-0.05	-3.00
STORM END	-1.95	-0.78	▓	0.20	0.35	-2.50	-0.53	▓	0.62	1.15

Table 4.2. Mean NOGAPS 48-h forecast error (F-A) for the five track types of characteristics. Sample includes 60 matching analysis and forecast storms.

Finally, a linear regression applied to the scatter diagram of synoptic-scale C_D, calculated using Equation 4.3, versus 1000-mb and 925-mb average winds for the 48-h forecast storms (Figure 4.21) exhibits a significant negative slope much like that found with the analysis storm data (Figure 4.13). Once again, given the assumptions used to calculate C_D, this indicates that other processes are offsetting the effects of friction. Therefore we can not say all processes affecting cyclones during cyclolysis are equally active in the analyses and forecasts, they do appear to combine to produce similar resulting decay rates.
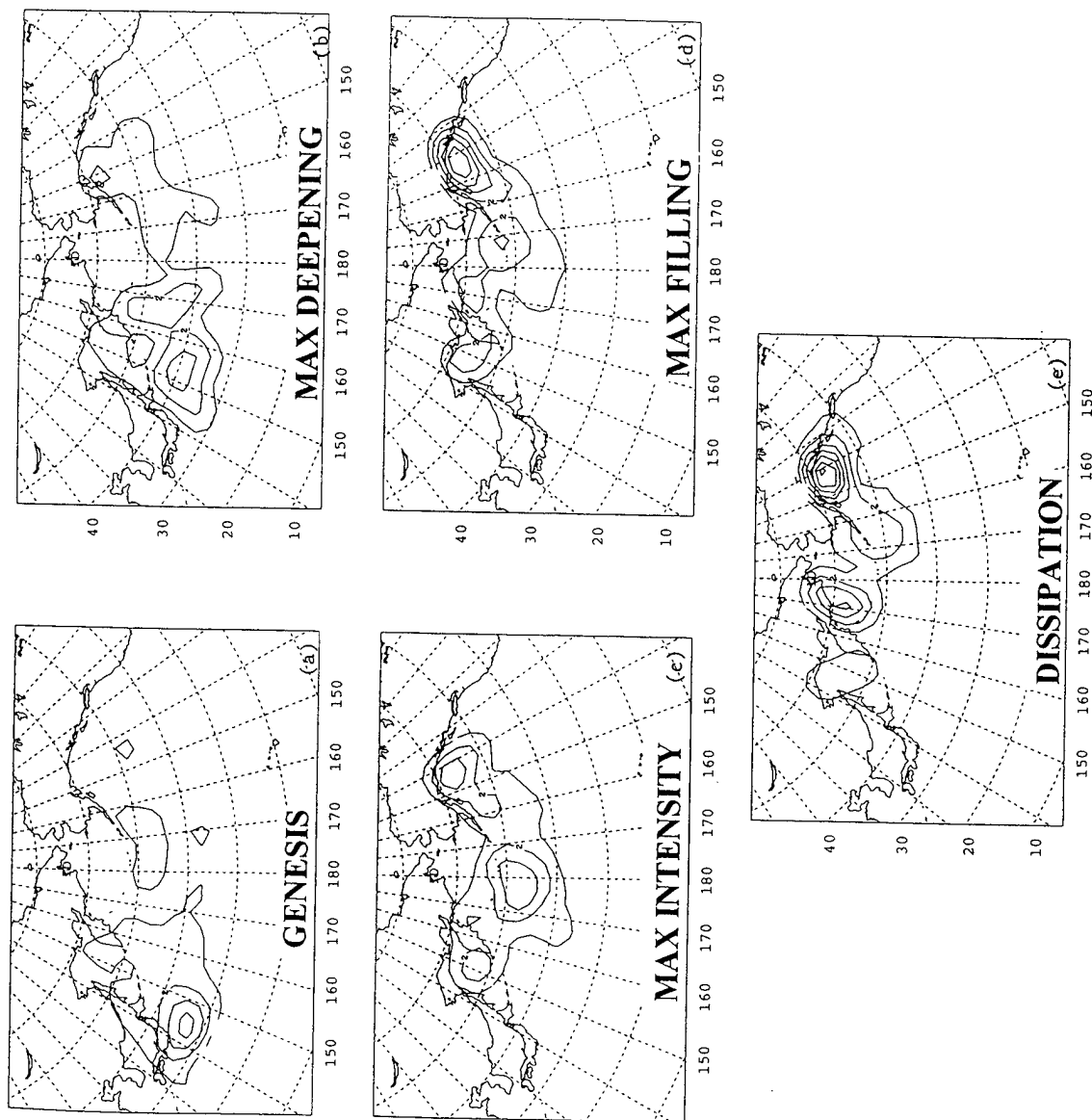
Figure 4.1. NOGAPS analysis North Pacific frequency (per 14 months) distribution of (a) cyclone genesis, (b) cyclone maximum deepening, (c) cyclone maximum intensity, (d) cyclone maximum filling, and (e) cyclone dissipation. The frequencies are for 5° latitude by 5° longitude boxes normalized to 42.5° latitude.

37
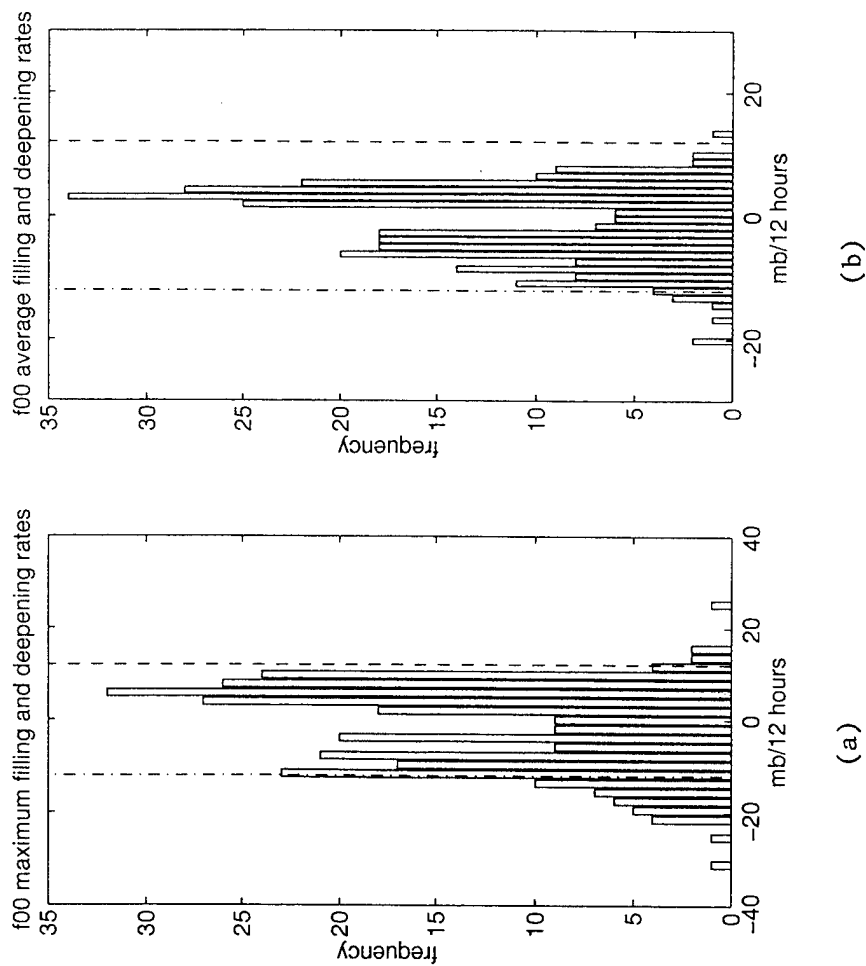
Figure 4.2. Histograms of NOGAPS analysis maximum (a) and average (b) deepening/filling rates [mb(12h)$^{-1}$]. Deepening "bombs" are less than -12 mb/12 hours (dashed-dotted lines) and filling "anti-bombs" are greater than 12 mb/12 hours (dashed lines). The pressure tendencies are normalized to 42.5° latitude.
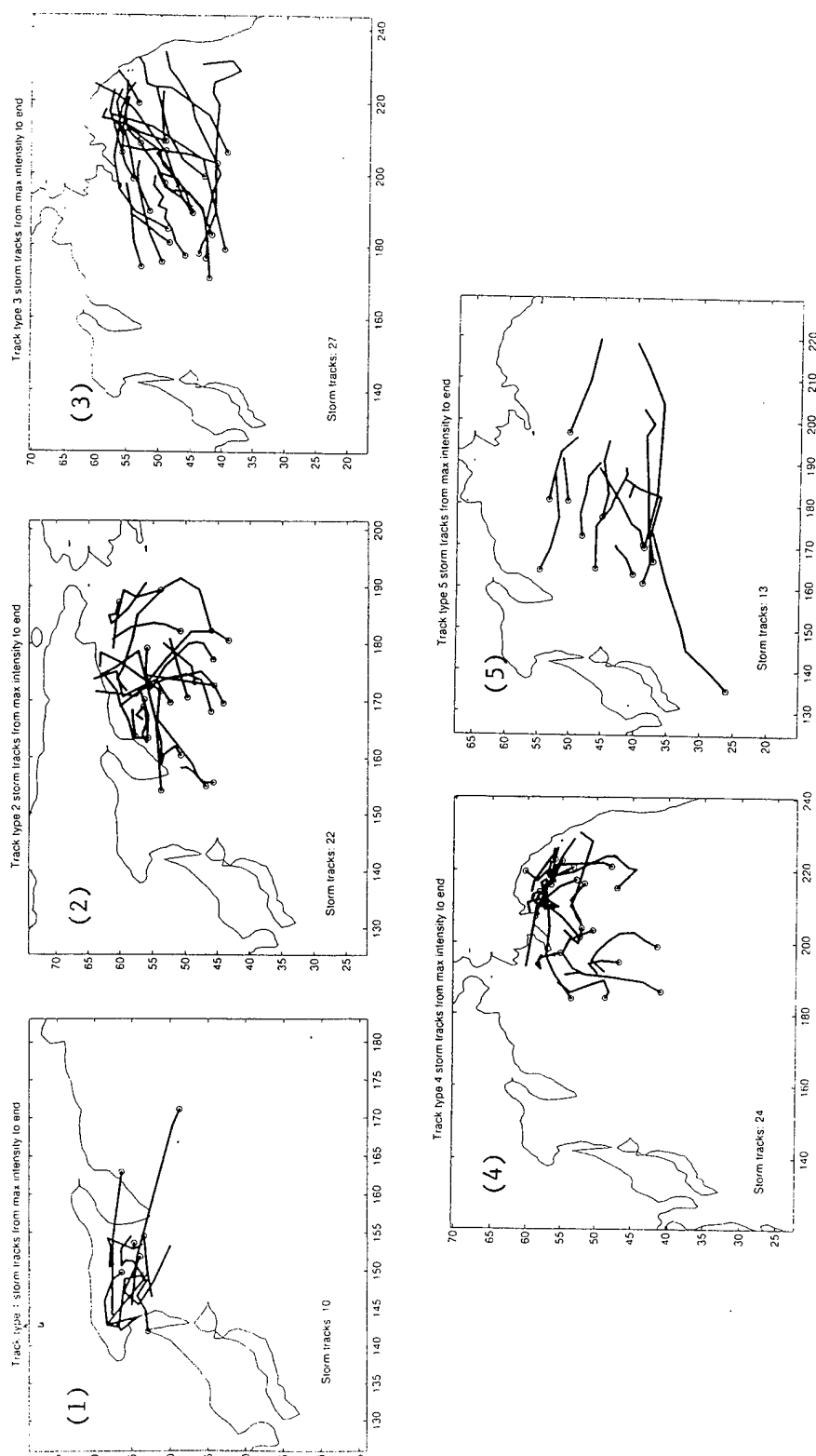
Figure 4.3. NOGAPS analysis cyclone track types (1-5) based on inferred North Pacific synoptic flow patterns. Only the decay portion of the tracks from maximum intensity (circled point) to storm end are shown. The number of storms in each category is listed in the lower left corner.
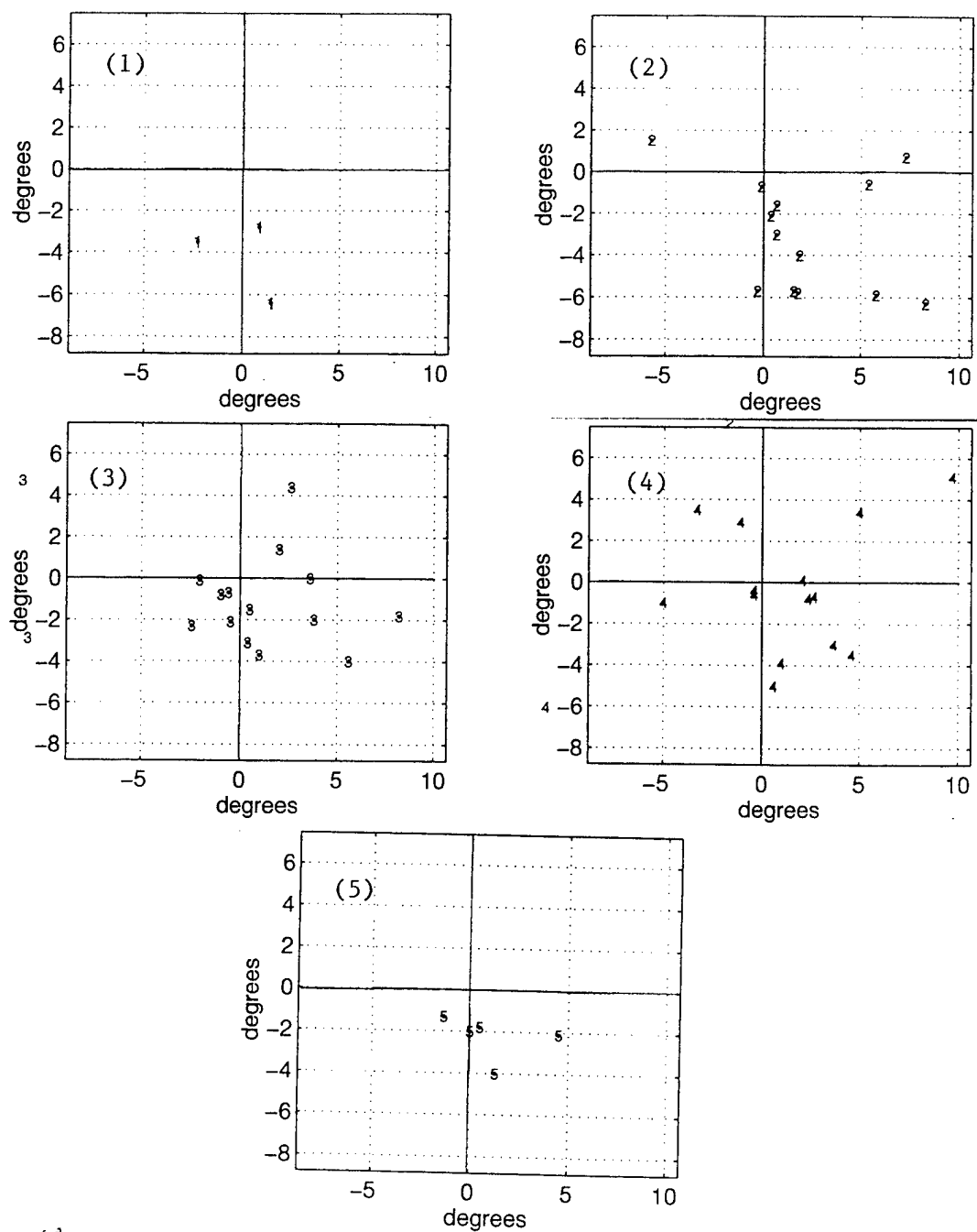
Figure 4.4. Horizontal offsets (degrees latitude) of the 500-mb lows in relation to corresponding surface lows in the NOGAPS analysis at the time of maximum cyclone intensity for the five track types. The location of the surface low is at 0,0.
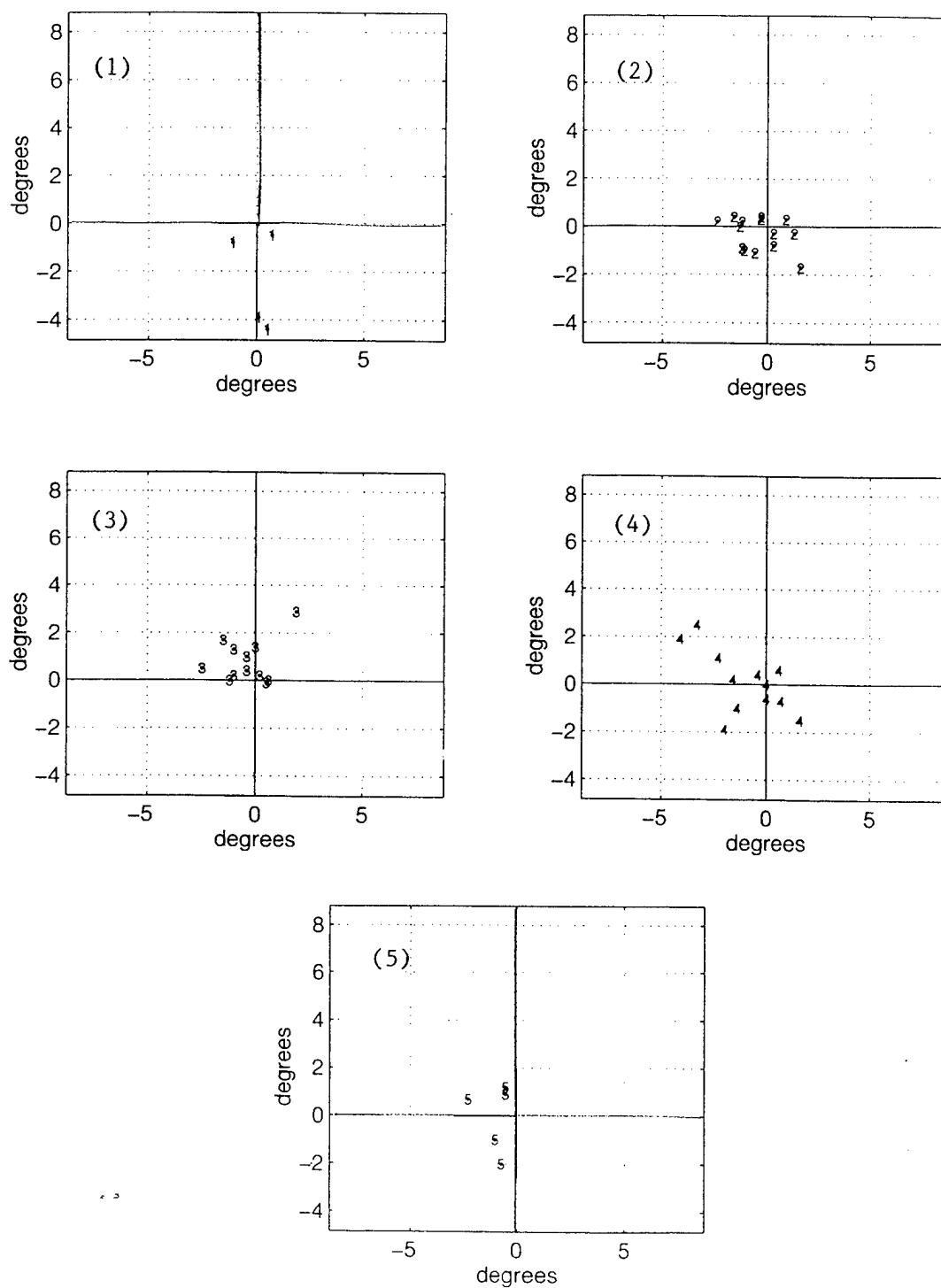
Figure 4.5. As in figure 4.4, except for 200-mb temperature maximum offsets.
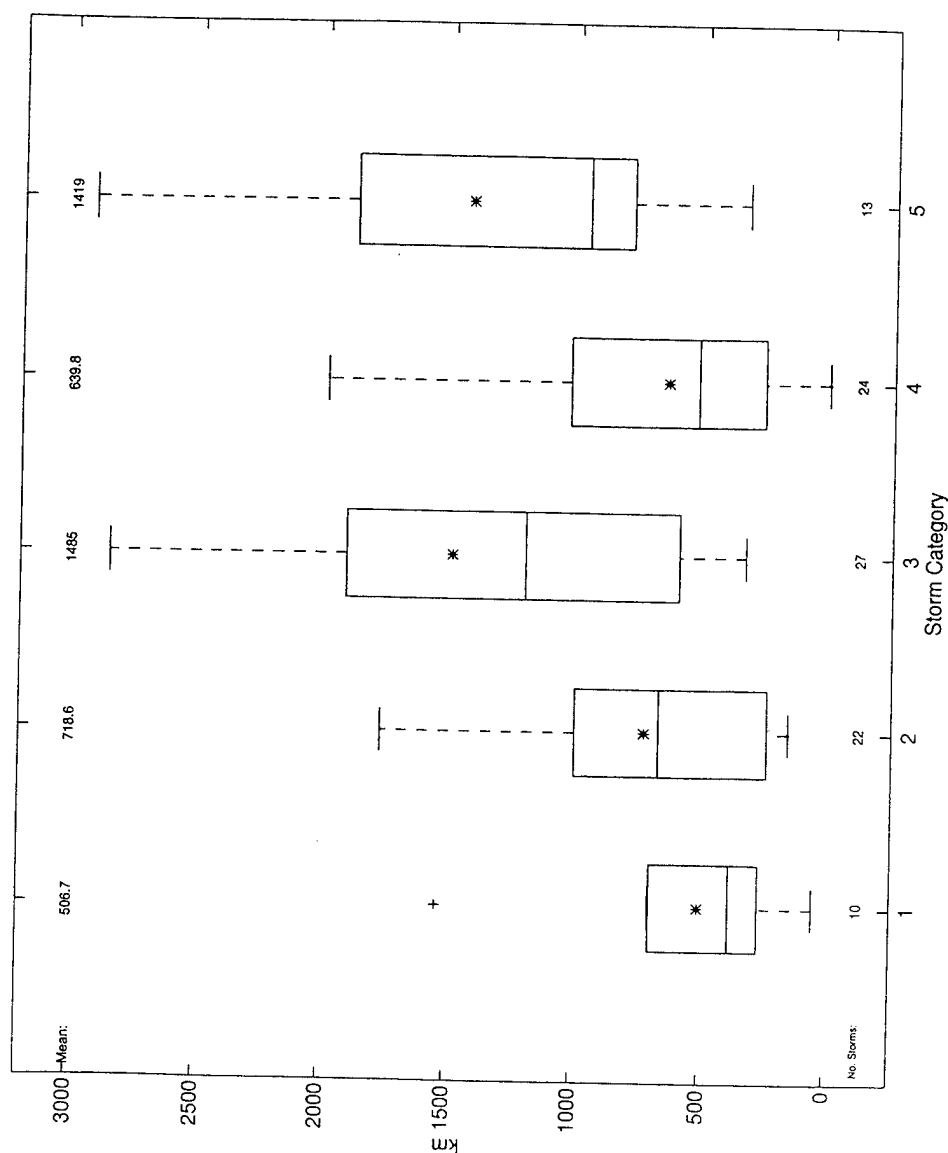
Figure 4.6. Analysis track type boxplots of fill translational distance. Ordinate represents fill distance in kilometers (km). Abscissa numbers represent track types. Boxplots indicate grouping of data values. The lower boundary of each box marks the 25th percentile and the upper boundary marks the 75th percentile. The upper dashed line extends to the upper adjacent value that is less than or equal to the 75th percentile plus 1.5 times the range of the middle 50% of the data. The lower dashed line extends to the lower adjacent value that is greater than or equal to the 25th percentile plus 1.5 times the range of the middle 50% of the data. Horizontal line in box defines the median, while the (*) defines the mean, and the (+) represents extreme values. Means are also shown on top of plot for each category while data sample numbers are at the bottom.
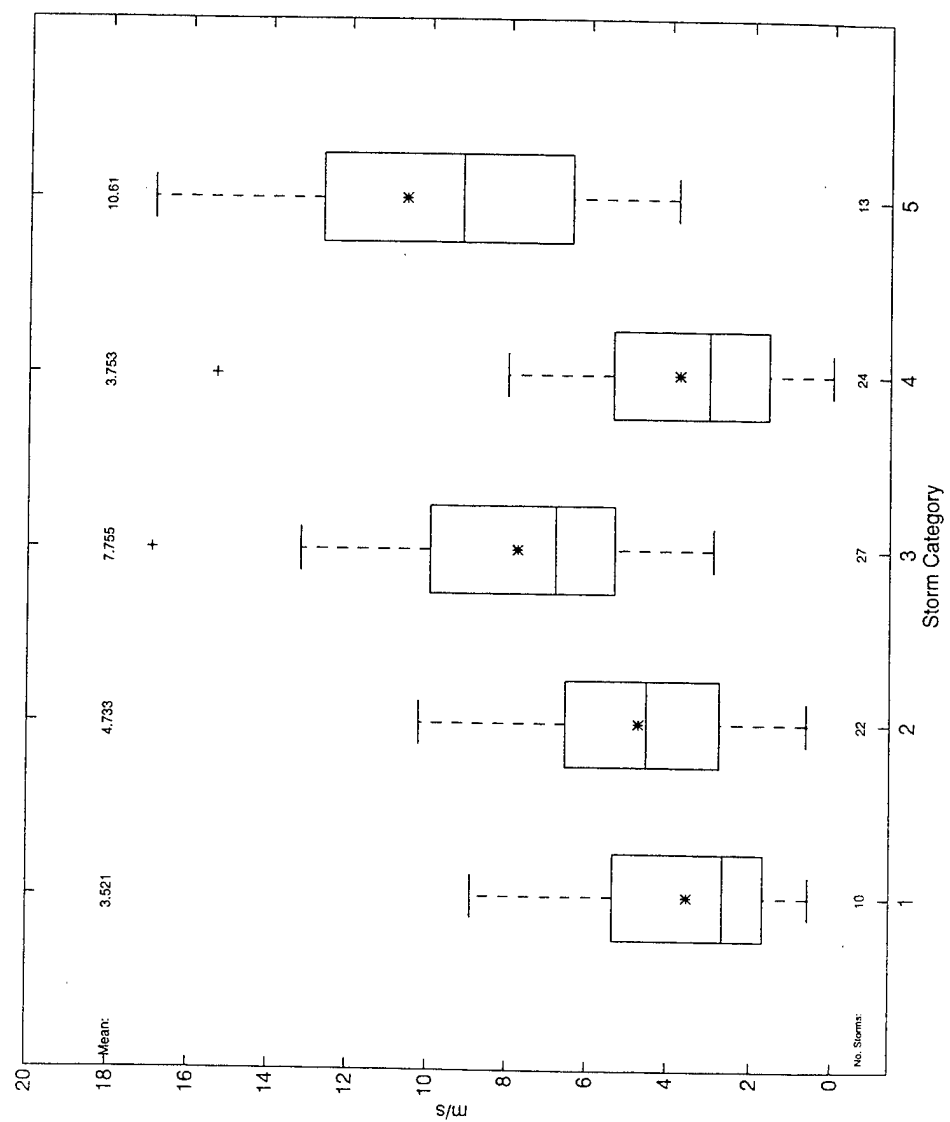
Figure 4.7. As in figure 4.6, except for average fill translational speed (m/s).
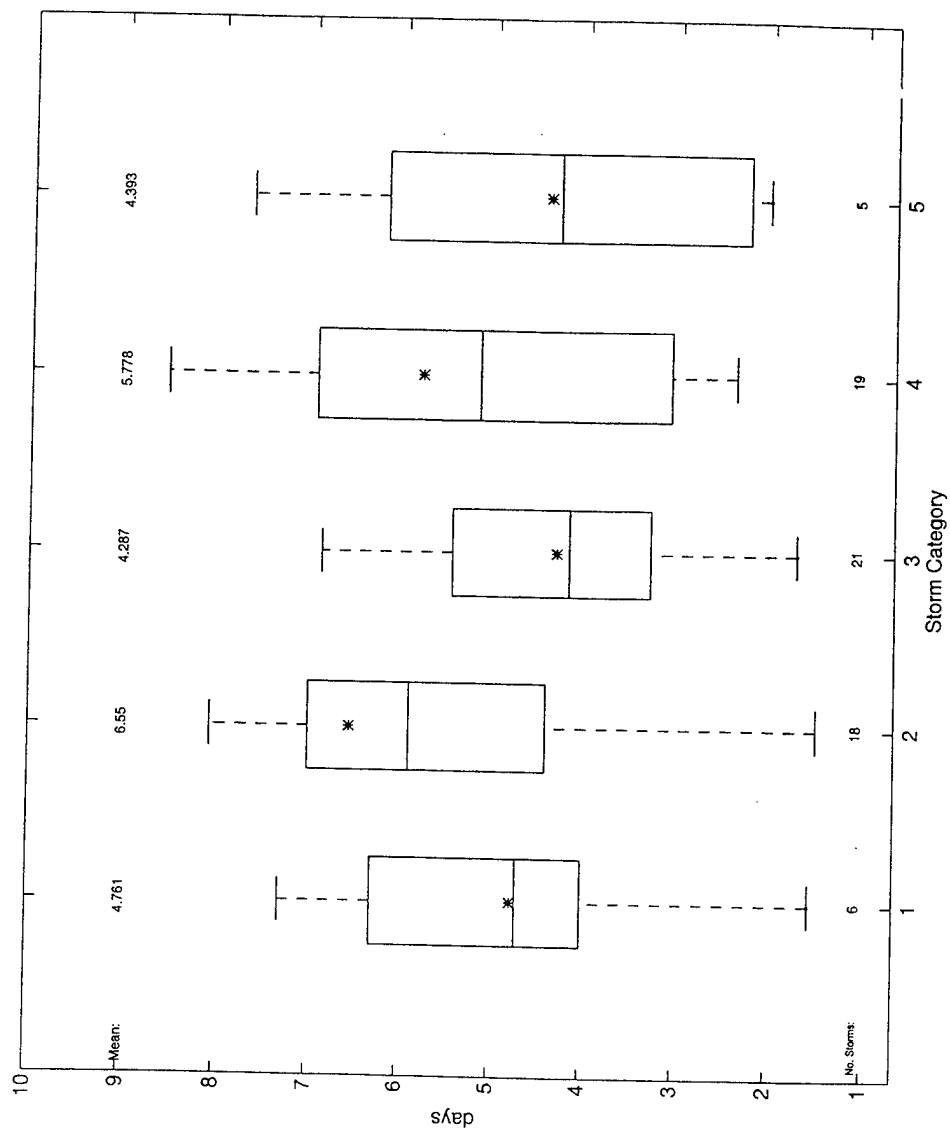
Figure 4.8. As in figure 4.6, except for fill average e-folding time (days).

44
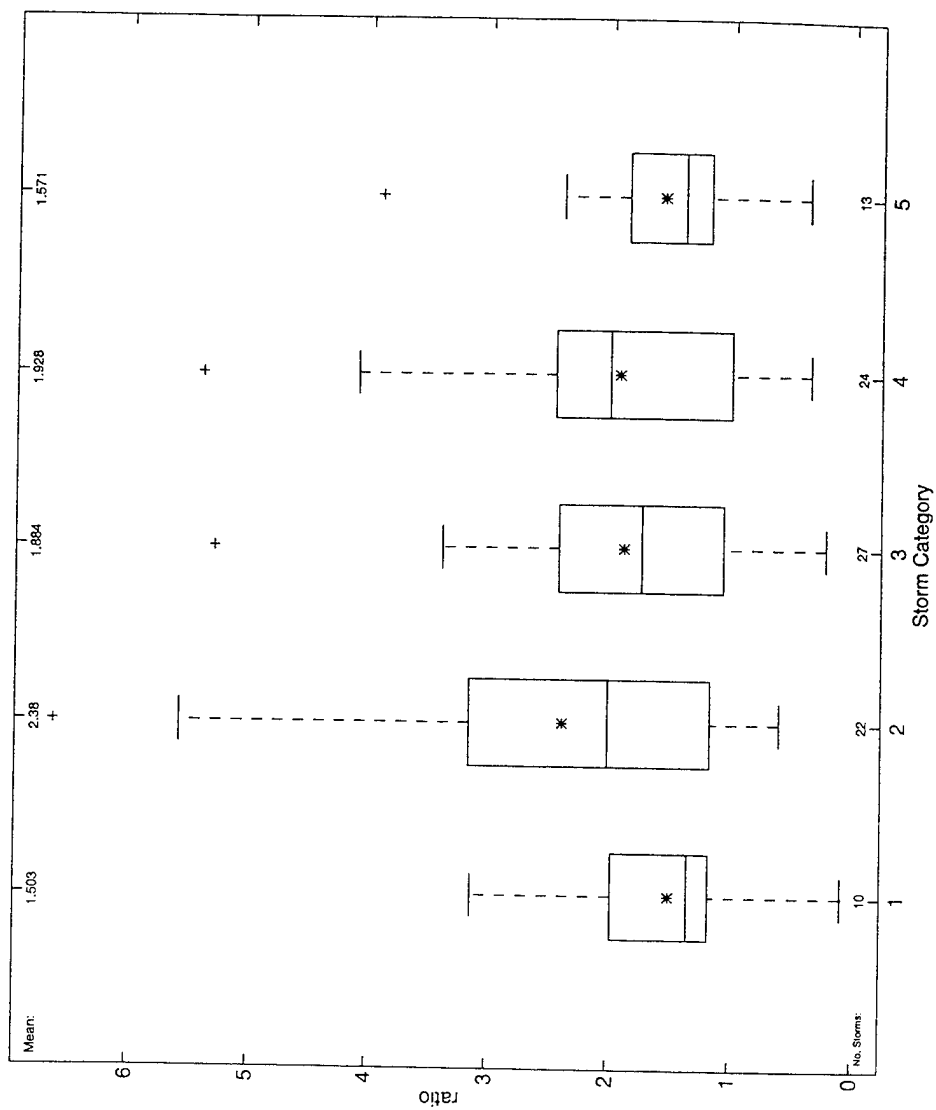
Figure 4.9. As in figure 4.6, except for average deepening rate/fill rate ratio (ratio).
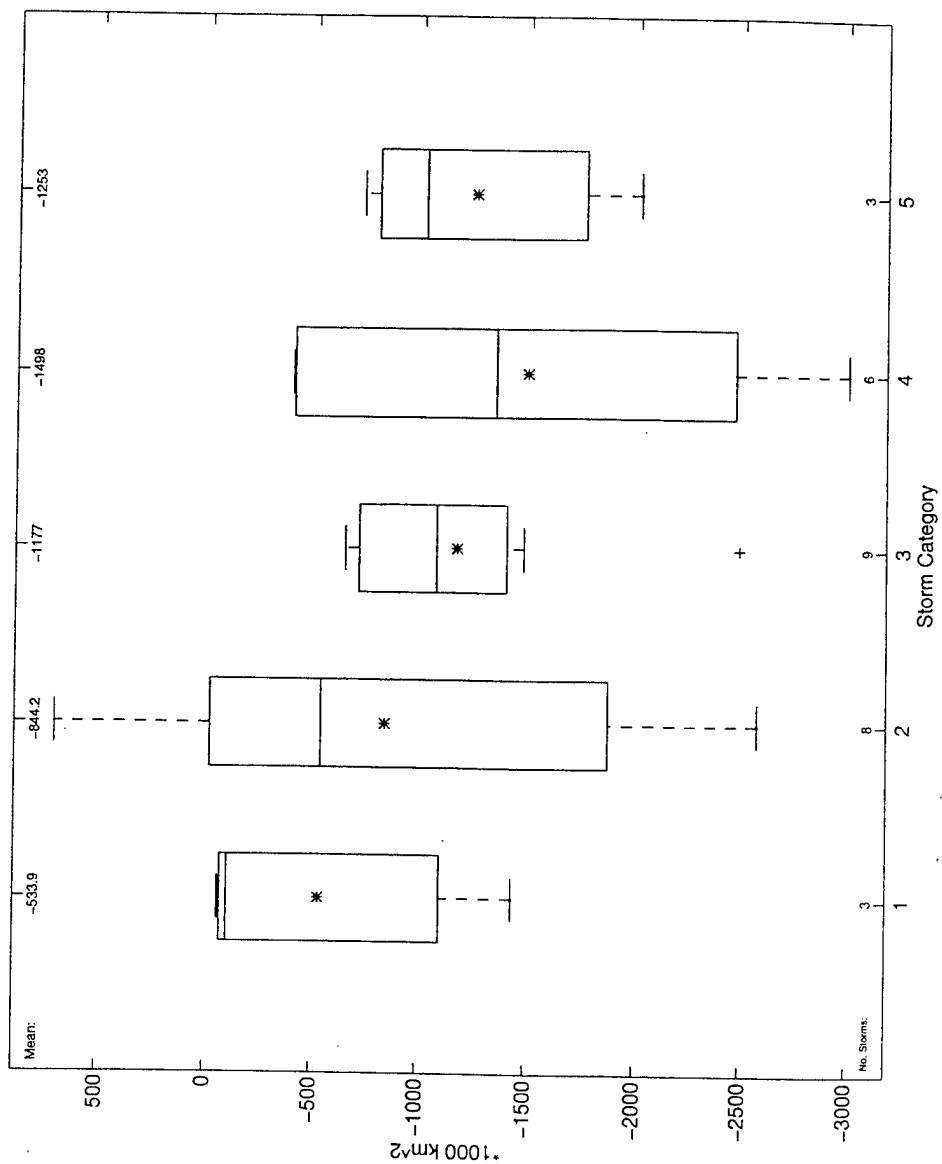
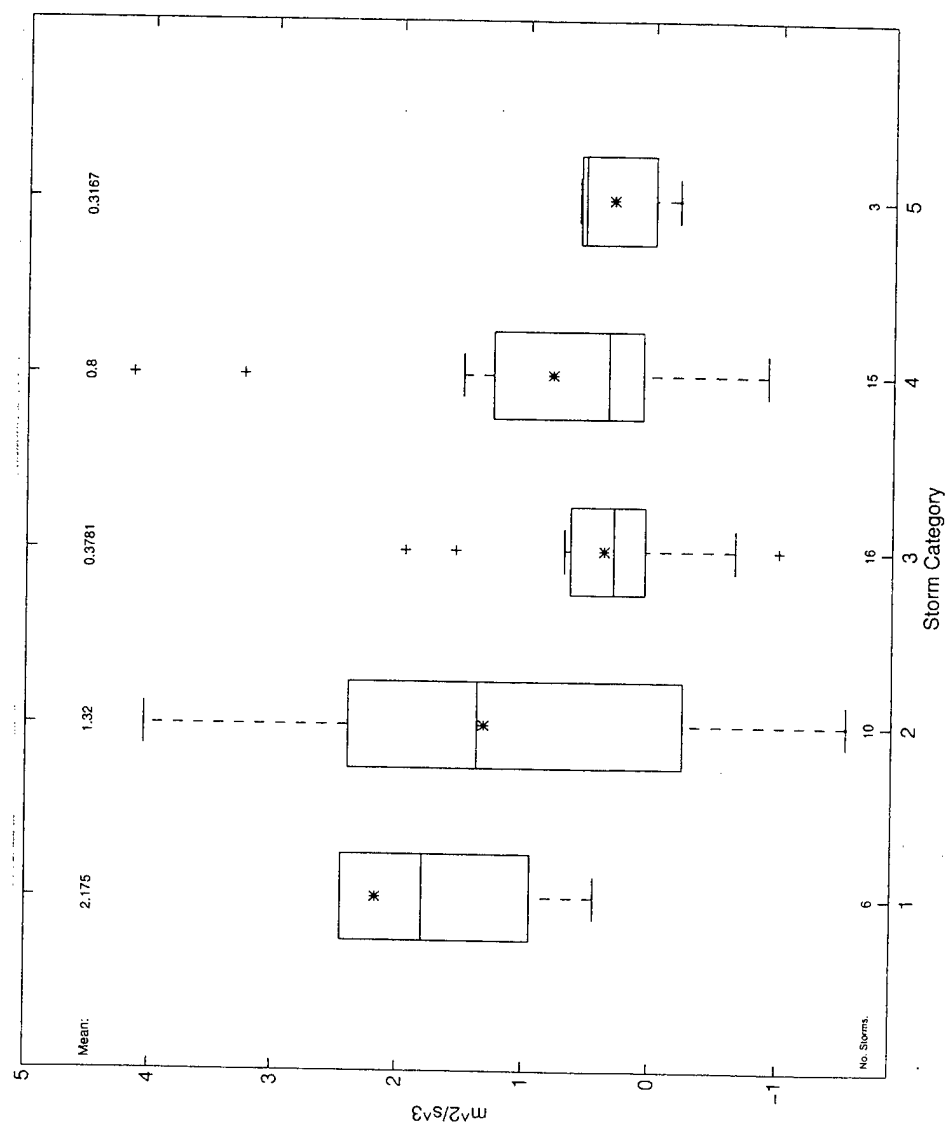Figure 4.10. As in figure 4.6, except for gale area from maximum intensity to the end of the storm ($*1000$ km^2).

46

Figure 4.11. As in figure 4.6, except for average barotropic energy conversion averaged from maximum intensity to storm end (m^2/s^3).
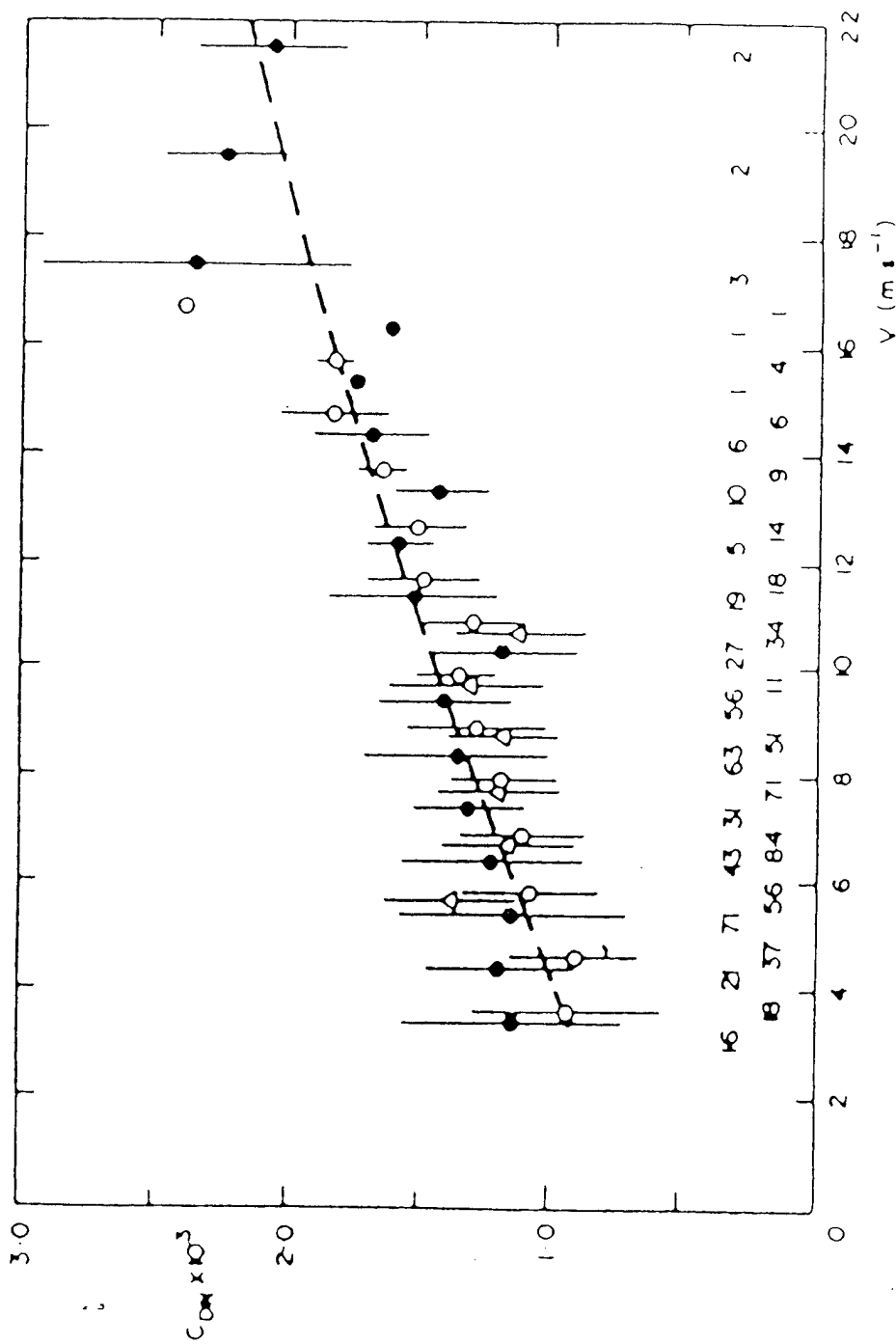
Figure 4.12. Neutral drag coefficient (C_D) values as a function of wind speed at 10 meter height. Mean values are shown for 1 m/s intervals based on the eddy correlation method (●) and wind profile method (○); wind profile data are also shown (△). Vertical bars refer to the standard deviation of individual data for each mean, with the number of data used in each 1 m/s interval shown abbove the abscissa axis: top line refers to (●), bottom line to (○). The dashed curve represents the variation of C_{DN} with V. (Garratt, 1977)
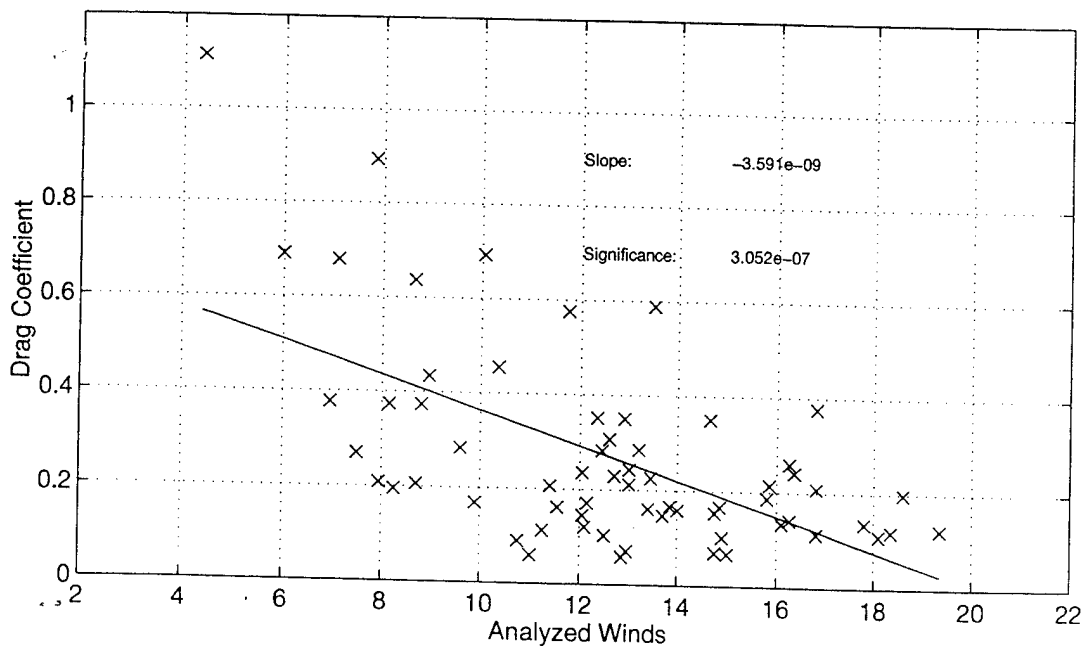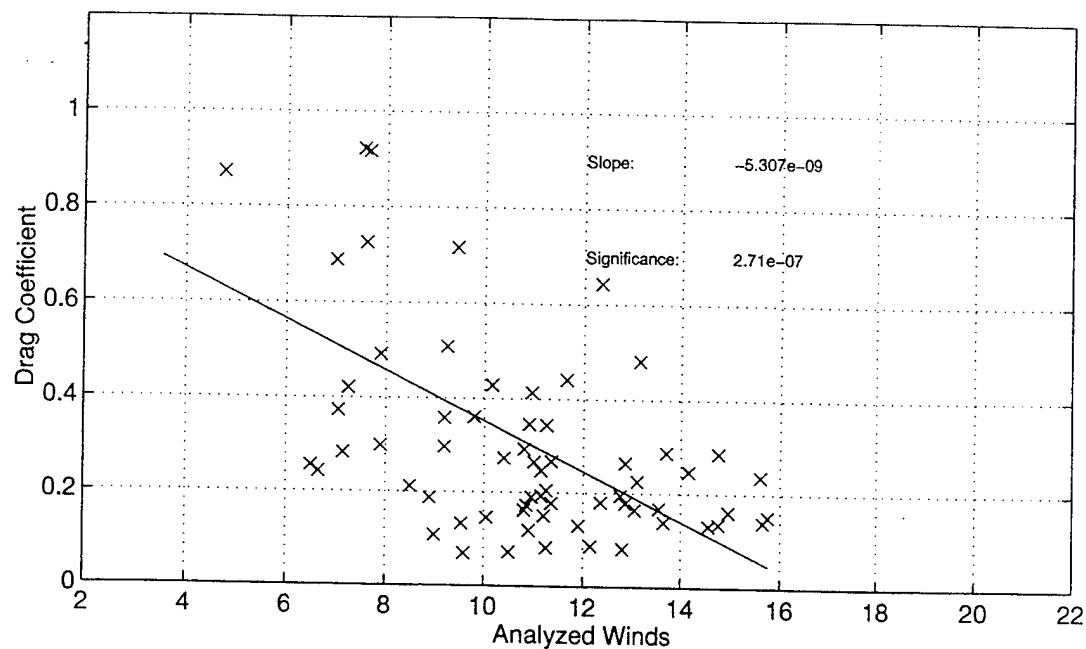
Figure 4.13. NOGAPS analysis drag coefficients (C_D) as a function of a) 1000 mb and b) 925 mb analyzed winds. Linear regression line defines an inverse relationship between C_D and winds. The low significance values indicate a very small probability that the linear relationship is due to chance.
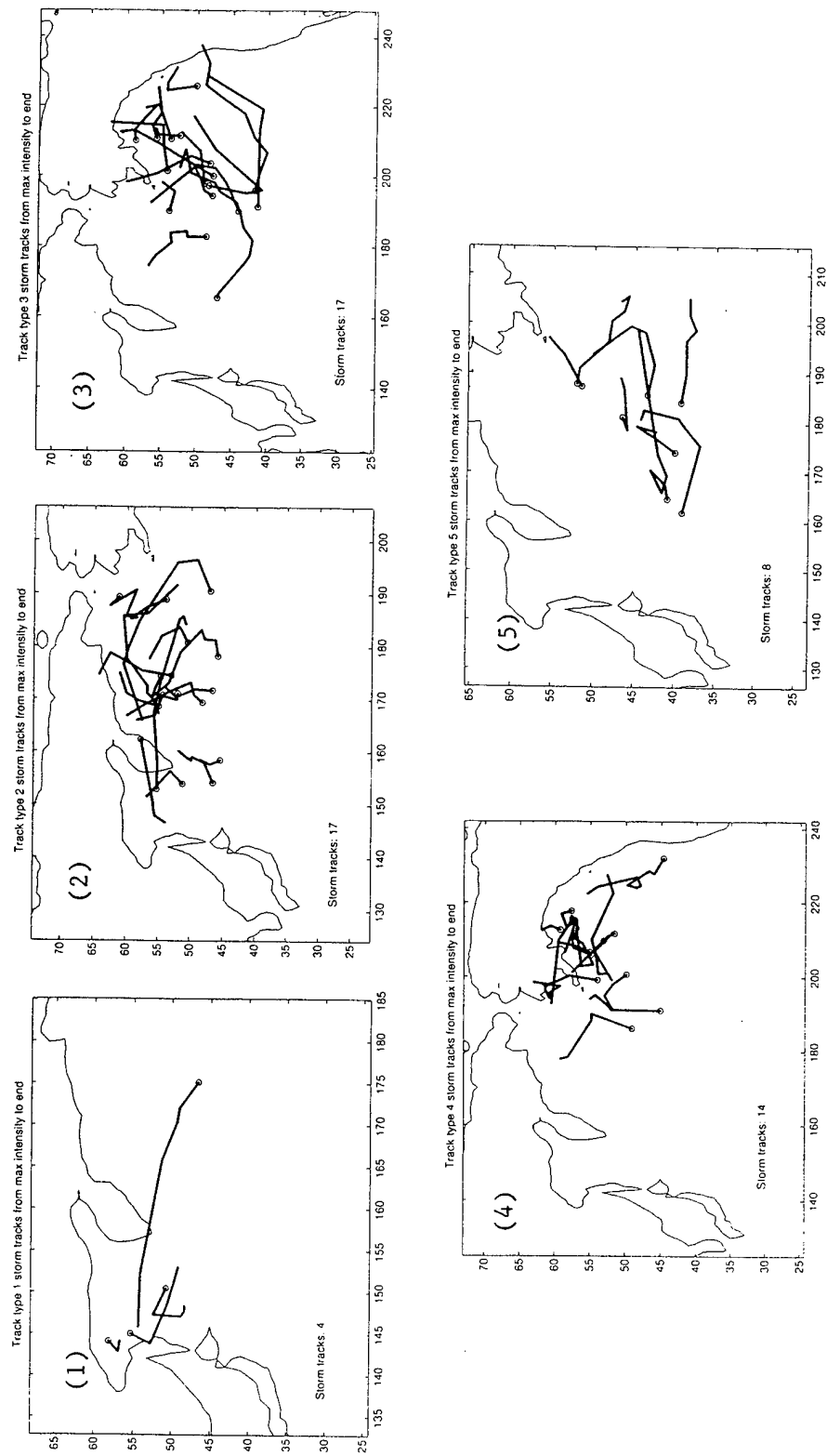
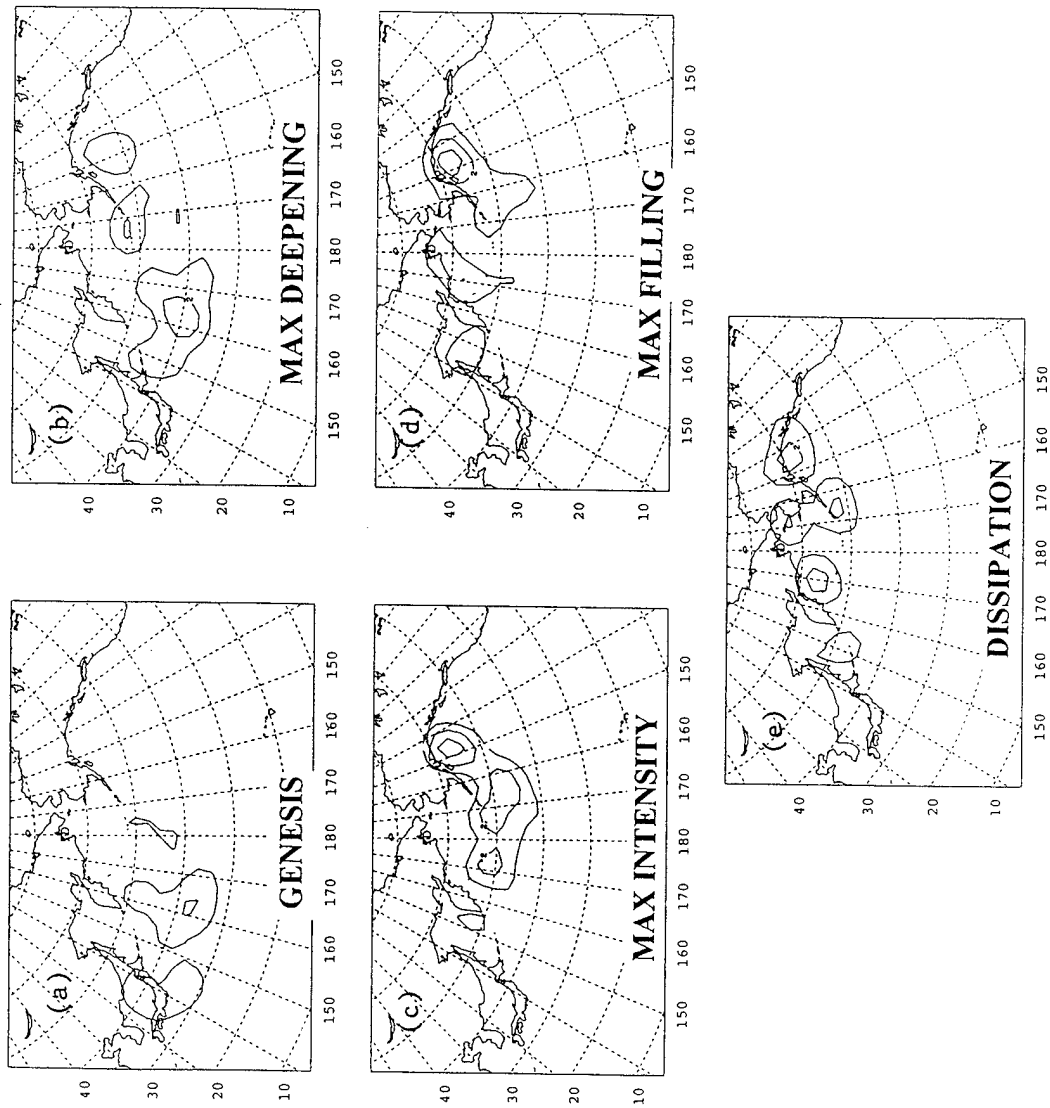Figure 4.14. As in figure 4.3, except for NOGAPS 48-h forecasts.

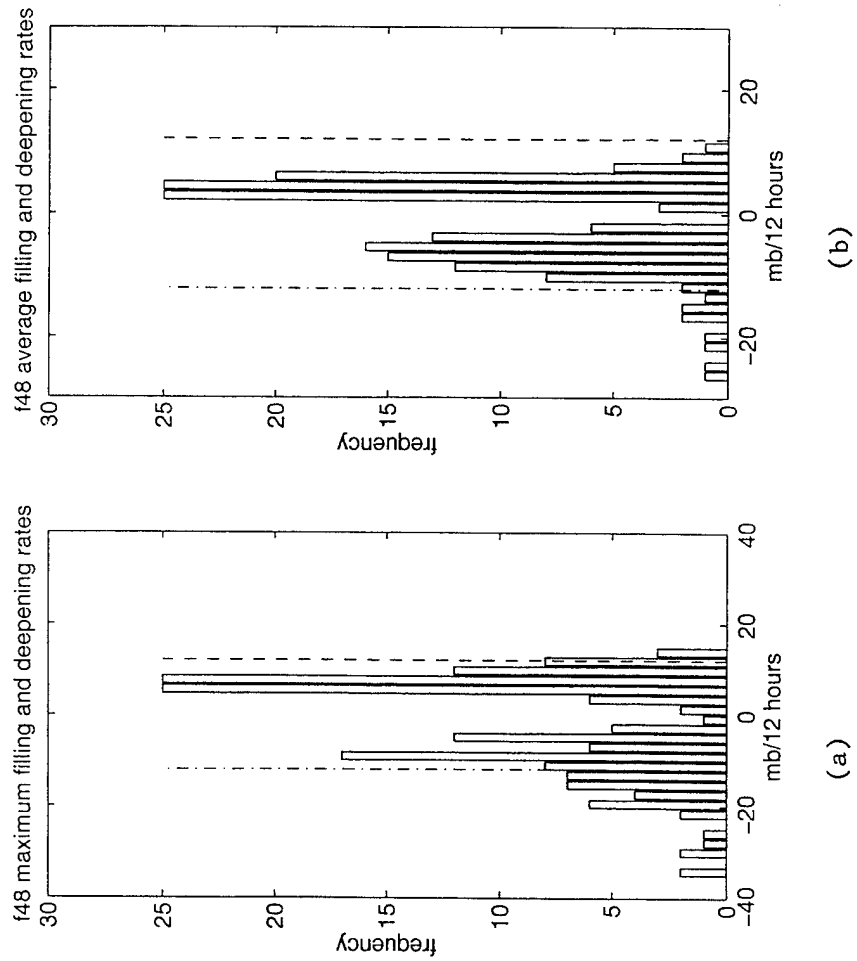Figure 4.15. As in figure 4.1, except for NOGAPS 48-h forecasts.

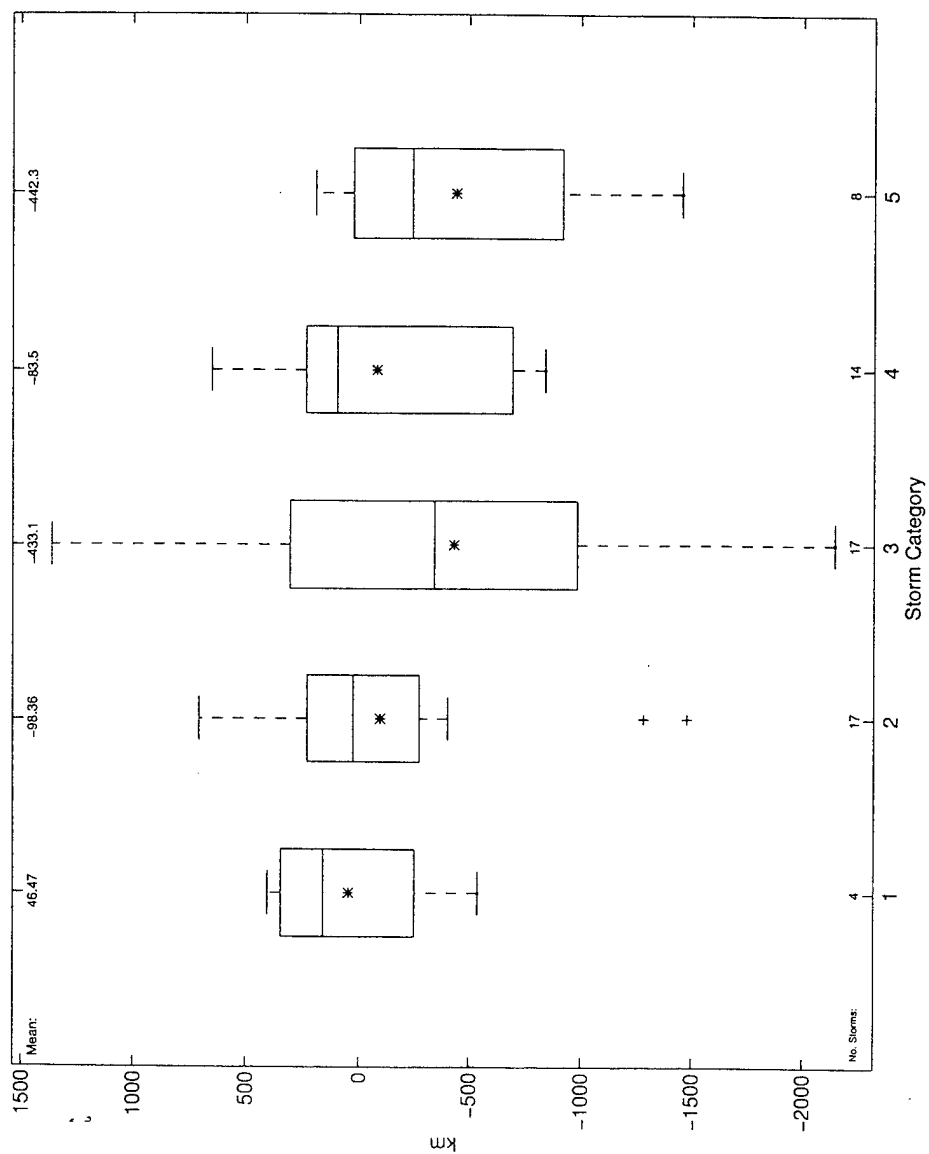Figure 4.16. As in figure 4.2, except for NOGAPS 48-h forecasts.

Figure 4.17. 48-h forecast error (f48-f00) track type boxplots of fill translational distance. Ordinate represents fill distance in kilometers (km). Abscissa numbers represent track types. Boxplot characteristics are as defined in figure 4.6.
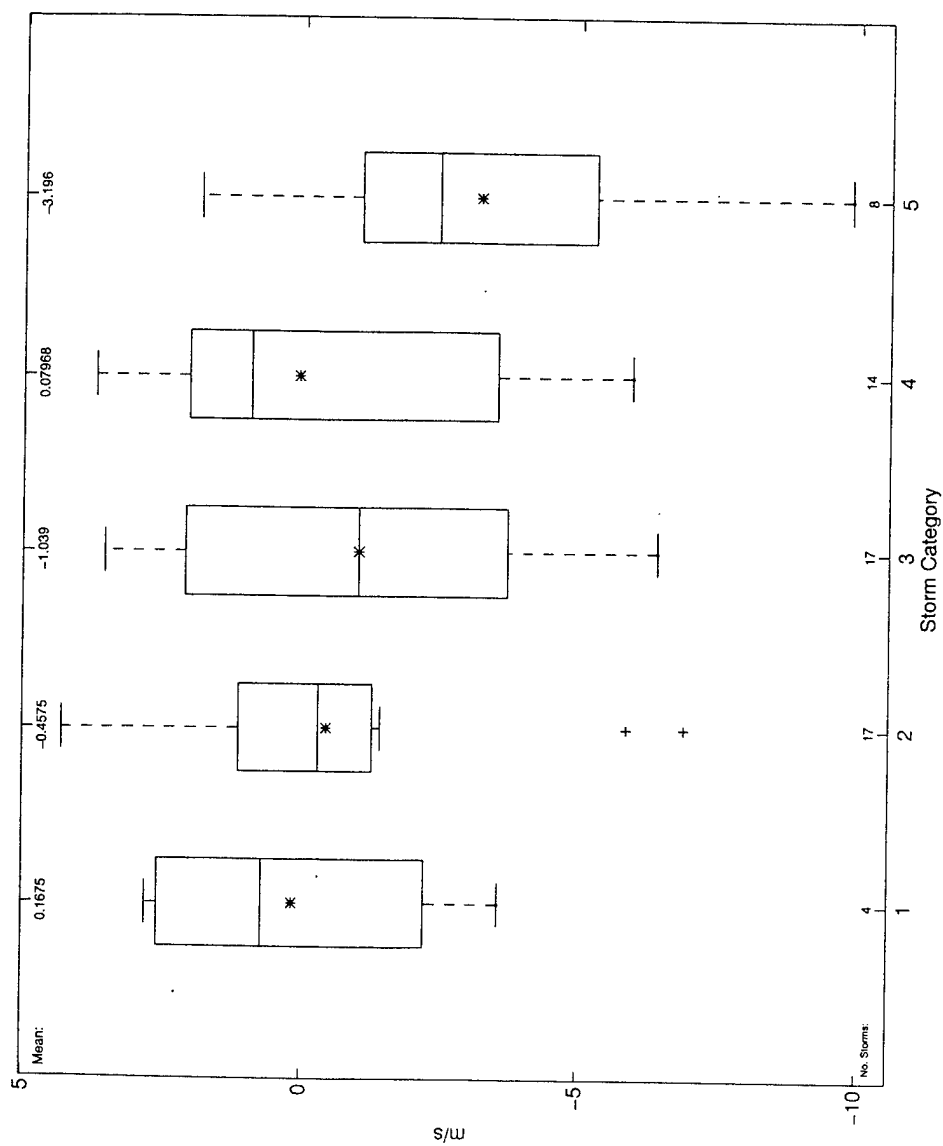
Figure 4.18. As in figure 4.17, except for fill translational speed error (m/s).
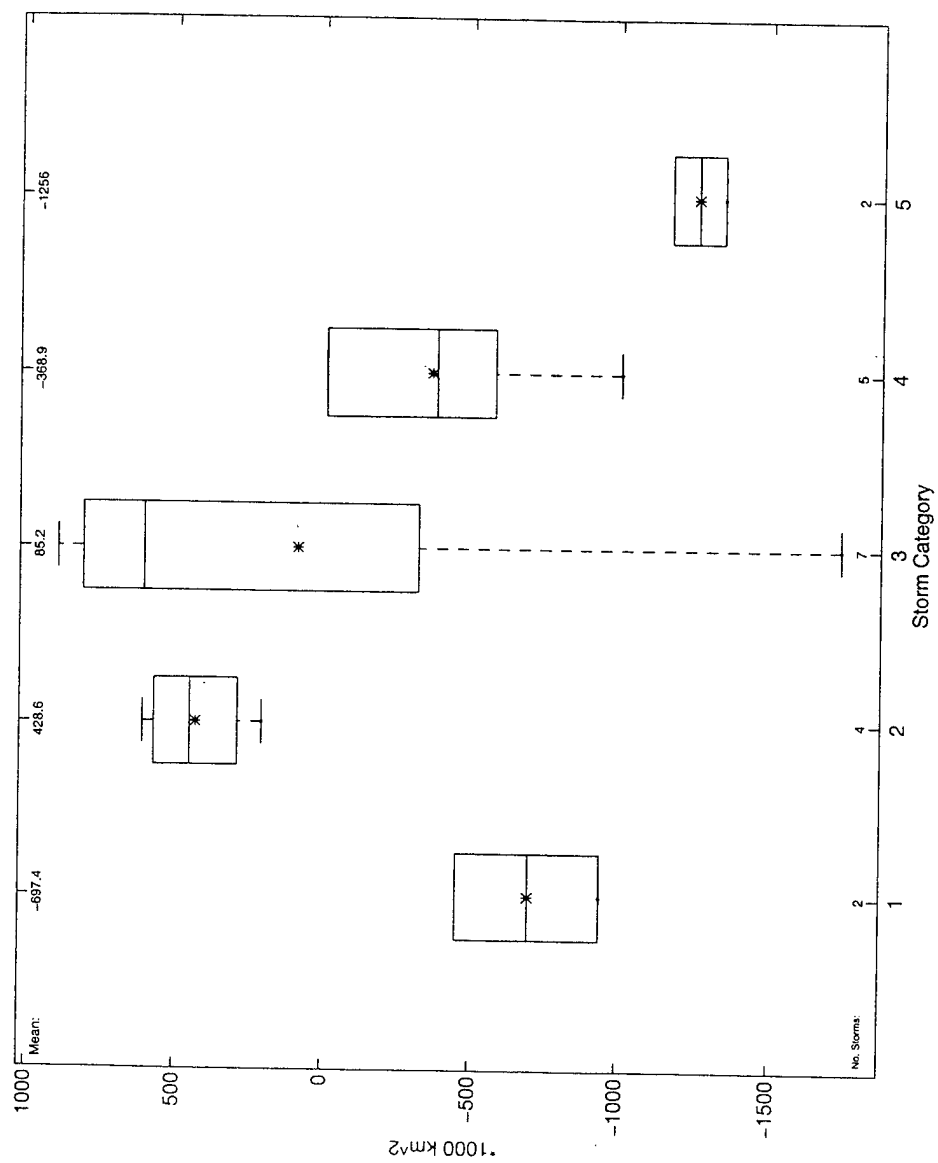
Figure 4.19. As in figure 4.17, except for forecast gale area at maximum intensity error (km²).
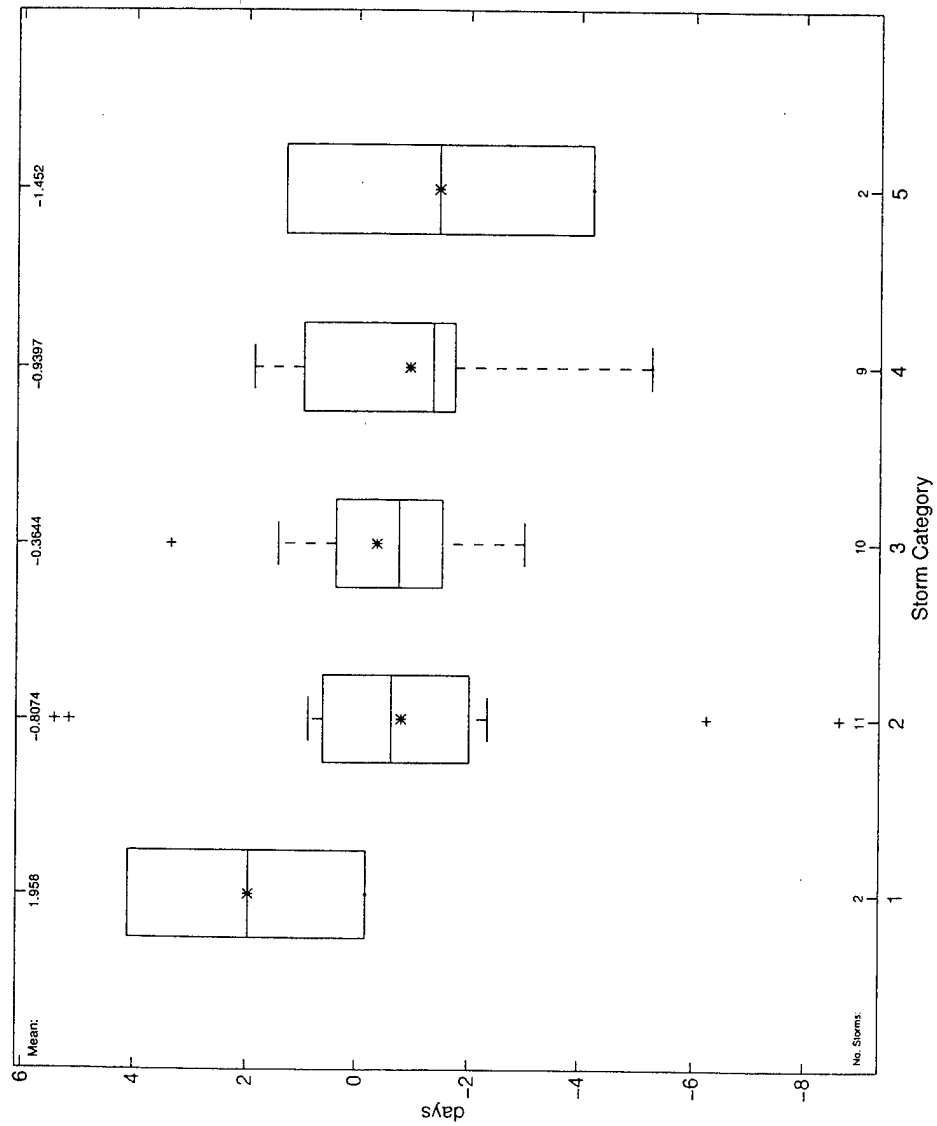
Figure 4.20. As in figure 4.17, except for forecast average e-folding error (days).
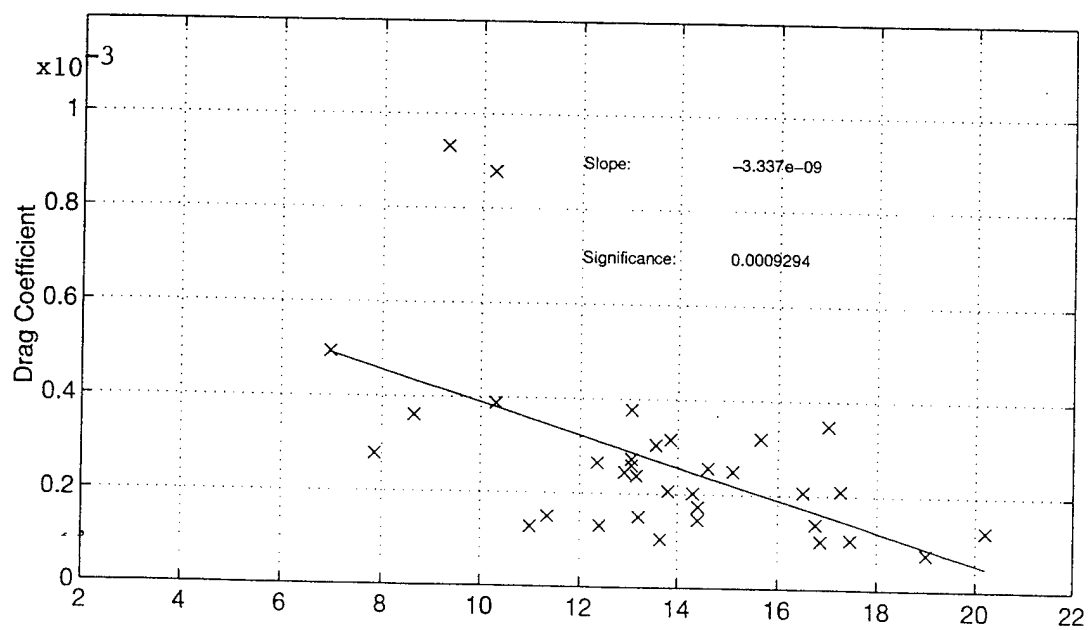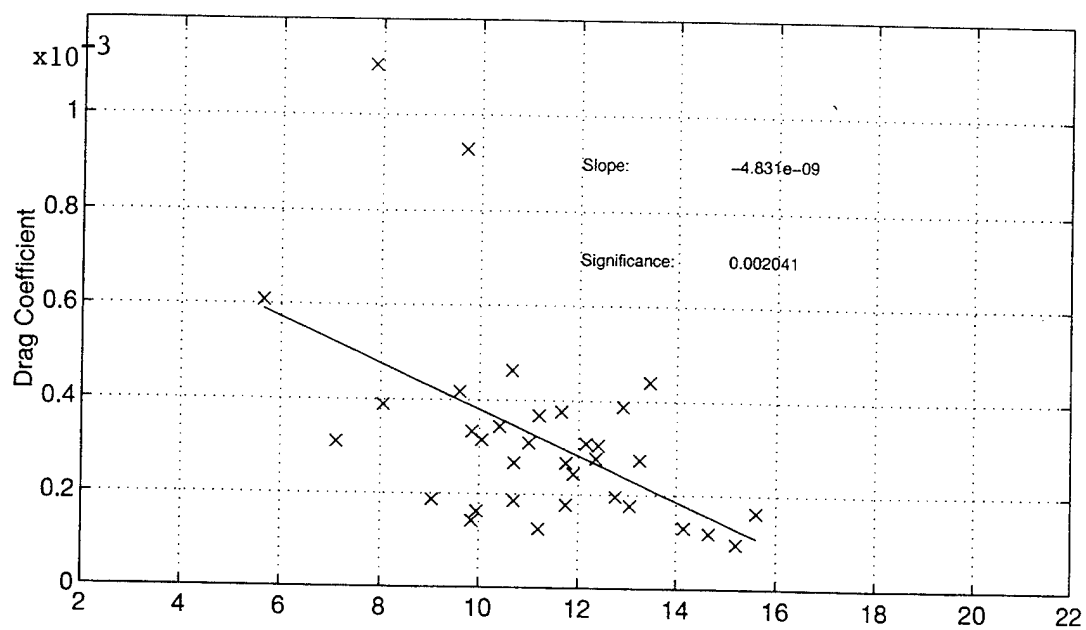
Figure 4.21. As in figure 4.13, except for NOGAPS 48-h forecasts.

V. CONCLUSIONS AND RECOMMENDATIONS

A. CONCLUSIONS

In this thesis, characteristics of cold-season cyclolysis in NOGAPS analyses and 48-h forecasts over the North Pacific Ocean have been documented. Not surprisingly, most cyclones over this region dissipate in the semi-permanent low centers near the Kamchatka Peninsula and the Gulf and Alaska. The fill rates of these storms follow a normal distribution with a small percentage of them filling rapidly or at "anti-bomb" rates. When storms are segregated according to characteristic track types interesting differences emerge. Most significantly, fast zonally moving storms tend to fill at a faster rate than storms that move meridionally and become associated with the primary North Pacific lows.

One of the motivations for this study was to determine whether there were any systematic differences between analysis and forecast cyclone fill rates. Such differences, especially those in which analysis storms fill faster than forecast storms, might suggest inadequate frictional parameterization over the ocean. In particular, Janssen (1991) and Doyle (1995) find that wind-wave interactions can affect the evolution of mesoscale features associated with cyclogenesis and have suggested that the increased roughness and drag that result from these interactions might effect cyclolysis as well. However, no evidence is found in the present study to support the premise that the inclusion of wind-wave interaction is important to simulating cyclolysis in global models. Firstly, no significant underfilling rate errors are evident in the 48-h NOGAPS forecasts. If anything, there is a tendency for the 48-h NOGAPS to overfill occluding cyclones. Moreover, if a

wind-wave effect were operative, than the drag coefficient should increase with wind speed at a faster rate than is typically the case (Figure 5.1). Not only is no such increase in drag evident in either the analyses or forecasts, drag is actually forced to decrease with wind speed. This suggests that at the synoptic scales considered in this study other factors, in addition to frictional spin-down, are influencing cyclolysis.

B. RECOMMENDATIONS

Cyclolysis is a subject that has not been studied in the past as intently as cyclogenesis. Therefore, the results presented here have few precedents to be compared to. Certainly, a more complete study with a larger data base of storms including those in other ocean basins and over land should be performed to ascertain if these initial findings are robust. This study was particularly hindered by the lack of surface temperature and wind information. In the future, 10-m NOGAPS fields should be used in the determination of drag coefficients and other friction-related parameters. Higher resolution 1° NOGAPS fields would also improve reliability. More detailed statistical as well as individual case studies should continue on wind-wave effects on cyclones. The documentation that the 48-h NOGAPS handles cyclolysis relatively well is somewhat surprising. It would be interesting to see whether longer duration 72-h to120-h forecasts perform as well. Finally, the relationship between gale area and other cyclone characteristics is a relatively unexplored topic, which is operationally important and that merits further study.
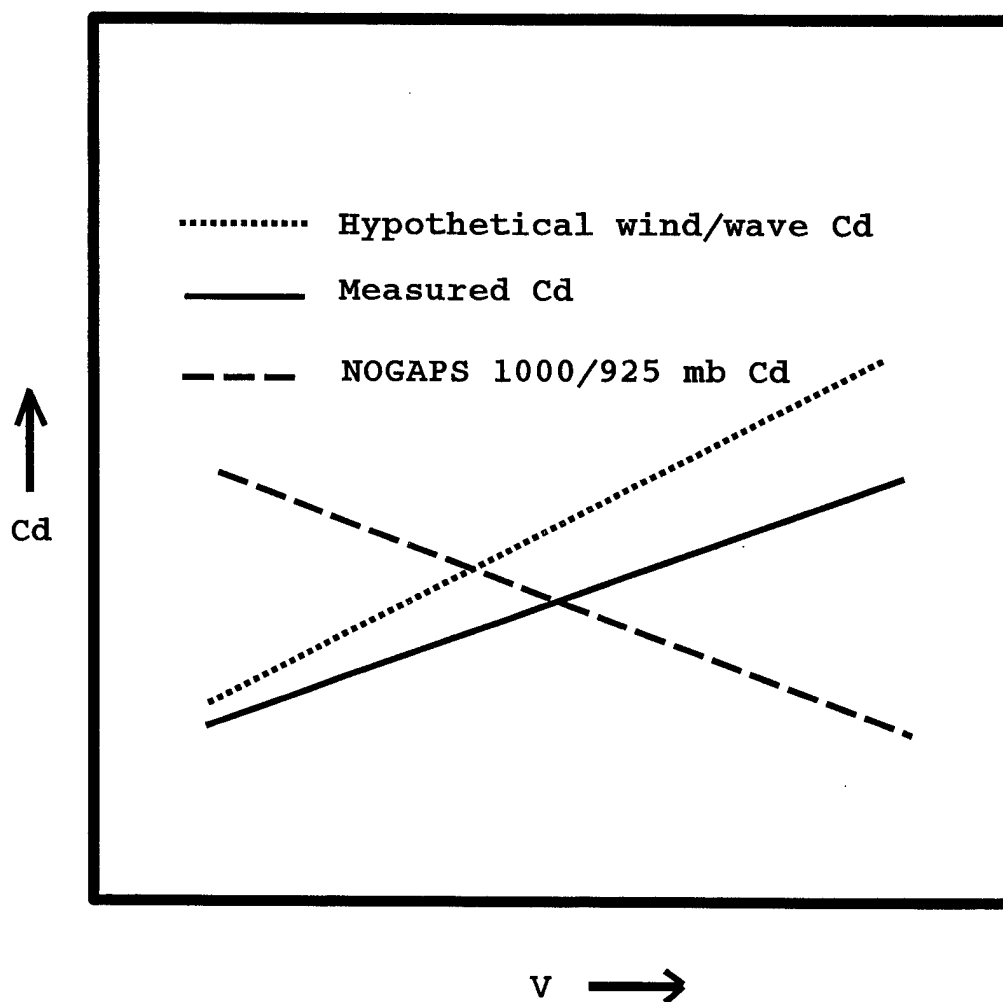
Figure 5.1. Schematic diagram of measured (solid line),
hypothetical wind-wave influenced (short-dashed line),
and NOGAPS synoptic (long-dashed line) drag coefficient
(Cd) versus wind speed (V).

LIST OF REFERENCES

Anthes, R. A. and Keyser, D., "Tests of a fine-mesh model over Europe and the United States", *Monthly Weather Review*, vol. 107, pp. 963-984, 1979

Bishop, C. H. and Thorpe, A. J., "Potential Vorticity and the Electrostatics Analogy: Quasi-geostrophic theory", *Quarterly Journal of the Royal Meteorological Society*, vol. 120, pp. 1397-1411, 1994

Bjerknes, J., *Geofysical Publikasjoner*, Norske Videnskaps-Akademie Oslo, Vol. I, No. 2, 1919

Bjerknes, J. and Solberg, H., *Geofysical Publikasjoner*, Norske Videnskaps-Akademie Oslo, Vol. II, No. 3, 1921

Bjerknes, J. and Solberg, H., *Geofysical Publikasjoner*, Norske Videnskaps-Akademie Oslo, Vol. III, No. 1, 1922

Carlson, T. N., *Mid-Latitude Weather Systems*, Harper Collins Academic, 1994

Charnock, H., "Wind Stress on the Water Surface", *Quarterly Journal of the Royal Meteorology Society*, vol. 81, pp. 639-640, 1955

Danard, M. B., "Numerical studies of effects of surface friction on large-scale atmospheric motions", *Monthly Weather Review*, vol. 97, pp. 835-844, 1969

Davis, C. A., and Emanuel, K. A., "Potential Vorticity Diagnostics of Cyclogenesis". *Monthly Weather Review*, vol. 119, pp. 1929-1953, 1991

Doyle, J. D., "Coupled ocean wave/atmosphere mesoscale model simulations of cyclogenesis", *Tellus*, vol. 47A, pp. 766-778, Monterey, CA, 1995

Farrell, B. F., "Unstable Baroclinic Modes Damped by Ekman Dissipation", Journal of Atmospheric Sciences, vol. 46, pp. 397-401, 1989

FNMOC, *Quarterly Performance Summary, Fall 1995*, Fleet Numerical Meteorological and Oceanography Center, vol. 10, num. 4, 1996

Gall, R., "Structural Changes of Growing Baroclinic Waves", *Journal of Atmospheric Sciences*, vol. 33, pp. 374-390, 1976

Garratt, J. R.,"Review of Drag Coefficients over Oceans and Continents", *Monthly Weather Review*, vol. 105, pp. 915-929, 1977

Graystone, P., "The introduction of topographic and frictional effects in a baroclinic model", *Quarterly Journal of the Royal Meteorological Society*, vol. 88, pp. 256-270, 1962

Gronas, S. and Shapiro, M. A., *The Life Cycles of Extratropical Cyclones, Vol. 1*, Aase Grafiske, 1994

Grumm, R. H., "Characteristics of Surface Cyclone Forecasts in the Aviation Run of the Global Spectral Model", *Weather and Forecasting*, vol. 8, pp. 87-112, 1993

Grumm, R. H. and Siebers, A. L., "Systematic Model Forecast Errors of Surface Cyclones in the NGM and AVN, January 1990", *Weather and Forecasting*, vol. 5, pp. 673-682, 1990

Gyakum, J. R., "On the Evolution of the QE II storm. Part I: Synoptic aspects", *Monthly Weather Review*, vol. 111, pp. 1137-1155, 1983

Gyakum, J. R., Anderson, J. R., Grumm, R. H., and Gruner, E. L.,"North Pacific Cold-Season Surface Cyclone Activity: 1975-1983", *Monthly Weather Review*, vol. 117, pp. 1141-1155, 1989

Haltiner, G. J. and Williams, R. T., *Numerical Prediction and Dynamic Meteorology, Second Edition*, Wiley & Sons, 1980

Harr, P. A., Elsberry, R. L., Hogan, T. F., and Clune, W. M., "Forecasts of North Pacific Maritime Cyclones with the Navy Operational Global Atmospheric Prediction System", Weather and Forecasting, vol. 7, pp. 456-467, 1992

Hirschberg, P. A. and Fritsch, J. M., "Tropopause undulations and the development of extratropical cyclones. Part I: Overview and observations from a cyclone event", *Monthly Weather Review*, vol. 119, pp. 496-517, 1991a

Hirschberg, P. A. and Fritsch, J. M., "Tropopause undulations and the development of extratropical cyclones. Part II: Diagnostic analysis and conceptual model", *Monthly Weather Review*, vol. 119, pp. 518-550, 1991b

Hogan, T. F., and Rosmond, T. E., "The description of the Navy operational global atmospheric prediction system's spectral forecast model". *Monthly Weather Review*, vol. 119, pp. 1786-1815, 1991

Holton, J. R., *An Introduction to Dynamic Meteorology, Third Edition.*, Academic Press, Inc., 1992

Hoskins, B. J., McIntyre, M. E., and Robertson, A. W., "On the use and significance of isentropic potential vorticity maps", *Quarterly Journal of the Royal Meteorological Society*, vol. 111, pp. 877-946, 1985

Janssen, P. E. M., "Quasi-linear Theory of Wind-Wave Generation Applied to Wave Forecasting", *Journal of Physical Oceanography*, vol. 19, pp. 745-754, 1991

Janssen, P. A. E. M., Lionello, P and Zambresky, L, "On the interaction of wind and waves", *Phil. Transcripts of the Royal Society of London*, vol. A329, pp. 289-301, 1989

Klein, W. H., "The Frequency of Cyclones and Anticyclones in relation to the mean circulation", *Journal of Meteorology*, vol. 15, pp. 98-102, 1957

Kuo, Y. H. and Reed R. J., "Numerical Simulation of an Explosively Deepening Cyclone in the Eastern Pacific", *Monthly Weather Review*, vol. 116, pp. 2081-2105, 1988

Mullen, S. L. and Smith, B. B., "An Analysis of Sea-level Cyclone Errors in NMC's Nested Grid Model (NGM) During the 1987-88 Winter Season", *Weather and Forecasting*, vol. 5, pp. 433-447, 1990

Mullen, S. L. and Smith, B. B., "An Evaluation of Sea Level Cyclone Forecasts Produced by NMC's NGM and Global Spectral Model", *Weather and Forecasting*, vol. 8, pp. 37-56, 1993

Newton, C. W. and Holopainen, E. O., *Extratropical Cyclones, The Erik Palmen Memorial Volume*, American Meteorological Society, 1990

Nordeng, T. E., "On the Wave Age Dependent Drag Coefficient and Roughness Length at Sea", *Journal of Geophysical Research*, vol. 96, pp. 7167-7174, 1991

Palmen, E. and Newton, C. W., *Atmospheric Circulation Systems, Their Stucture and Physical Interpretation*, Academic Press, 1969

Petterssen, S., *Weather Analysis and Forecasting, Volumes I & II*, McGraw-Hill Book Company, 1956

Reitan, C. H., "Frequencies of Cyclones and Cyclogenesis for North America, 1951-1970", Monthly Weather Review, vol. 102, pp. 861-868, 1974

Roebber, P. J., "Statistical Analysis and Updated Climatology of Explosive Cyclones". *Monthly Weather Review*, vol. 112, pp. 1577-1589, 1984

Sanders, F., "Explosive Cyclogenesis in the west-central North Atlantic Ocean, 1981-84", *Monthly Weather Review*, vol. 114, pp. 1781-1794, 1986

Sanders, F., "Skill of Operational Dynamical models in cyclone prediction out to five-days range during ERICA", *Weather and Forecasting*, vol. 7, pp. 3-25, 1992

Sanders, F and Auciello, E. P., "Skill in Prediction of Explosive Cyclogenesis over the Western North Atlantic Ocean", *Weather and Forecasting*, vol. 4, pp. 157-172, 1989

Sanders, F. and Gyakum, J. R., "Synoptic-Dynamic Climatology of the 'Bomb'", *Monthly Weather Review*, vol. 108, pp. 1589-1606, 1980

Simmons, A. J. and Hoskins, B. J., "The Downstream and Upstream Development of Unstable Baroclinic Waves", *Journal of Atmospheric Sciences*, vol. 36. pp. 1239-1254, 1979

Simmons, A. J. and Hoskins, B. J., "Barotropic Influences on the Growth and Decay of Nonlinear Baroclinic Waves", *Journal of Atmospheric Sciences*, vol. 37. pp. 1679-1684, 1980

Simons, T. J., "The Nonlinear Dynamics of Cyclone Waves", *Journal of the Atmospheric Sciences*, vol. 29, pp. 38-52, 1972

Smith, P. J., "The Energetics of Extratropical Cyclones", *Journal of Geophysical Research*, vol. 85, pp. 378-386, 1980

Stull, R. B., *An Introduction to Boundary Layer Meteorology*, Kluwer Academic Publishers, 1988

Ulbrich, U, Burger, G., Schriever, D., Von Storch, H., Weber, S. L., and Schmitz, G., "The effect of a regional increase in ocean surface roughness on the tropospheric circulation: a GCM experiment", *Climate Dynamics*, vol. 8, pp. 277-285, 1993

Whittaker L. M. and Horn, L. H., "Geographical and Seasonal Distribution of North American Cyclogenesis", 1958-1977", *Monthly Weather Review*, vol. 109, pp. 2312-2322, 1981

Zishka, K. M. and Smith, P. J., "The Climatology of Cyclones and Anticyclones over North America and Surrounding Ocean Environs for January and July, 1950-77", *Monthly Weather Review*, vol. 108, no. 4, pp. 387-401, Purdue University, 1980

INITIAL DISTRIBUTION LIST

1.   Defense Technical Information Center   2
8725 John J. Kingman Rd., STE 0944
Ft. Belvoir, VA 22060-6218

2.   Dudley Knox Library   2
Naval Postgraduate School
411 Dyer Rd.
Monterey, CA 93943-5101

3.   Oceanography Department   1
Code OC/CO
Naval Postgraduate School
589 Dyer Rd Rm 252
Monterey, CA 93943-5122

4.   Meteorology Department   1
Code MR/Hy
Naval Postgraduate School
589 Dyer Rd Rm 252
Monterey, CA 93943-5122

5.   Dr. Paul A. Hirschberg   4
Code MR/Hs
Naval Postgraduate School
589 Dyer Rd Rm 252
Monterey, CA 93943-5122

6.   Dr. Patrick A. Harr   1
Code MR/Hr
Naval Postgraduate School
589 Dyer Rd Rm 252
Monterey, CA 93943-5122

7.   LT Tom P. Wojahn   2
1722 Center Groton Rd
Ledyard, CT 06339

8.   Dr. James D. Doyle   1
Naval Research Laboratory
7 Grace Hopper Ave. Stop 2
Monterey, CA 93943-5502

9.   Mr. William Clune   1
        Naval Research Laboratory
        7 Grace Hopper Ave. Stop 2
        Monterey, CA 93943-5502

10.   Commander   1
        Naval Meteorology and Oceanography Command
        1020 Balch Blvd.
        Stennis Space Center, MS 39529-5005

11.   Commanding Officer   1
        Naval Oceanographic Office
        Stennis Space Center, MS 39529-5001

12.   Commanding Officer   1
        Fleet Numerical Meteorology and
        Oceanographic Center
        7 Grace Hopper Ave. Stop 4
        Monterey, CA 93943

13.   Commanding Officer   1
        Naval Research Laboratory
        Stennis Space Center, MS 39529-5004

14.   Superintendent   1
        Naval Research Laboratory
        7 Grace Hopper Ave. Stop 2
        Monterey, CA 93943-5502